

# ELECTRONIC MATERIALS DIVISION

350 State Street, Pasadena, California 91109 (213) 796-8381

AD715454

NO CODE STAMP

## Indium Arsenide-Phosphide Injection Lasers

Contract No. H0001149-C-0413

Sponsored by Advanced Research Projects Agency

ARPA Order No. 306

FINAL TECHNICAL REPORT

October 1970

Office of Naval Research, Physics Branch  
Arlington, Va. 22217

D D C  
RECEIVED  
DEC 15 1970  
RECEIVED



BELL & HOWELL

Reproduced by  
NATIONAL TECHNICAL  
INFORMATION SERVICE

**INDIUM ARSENIDE-PHOSPHIDE INJECTION LASERS**

**Final Technical Report**

**Contract No. N00014-69-C-0415**

**Prepared by**

**Alan G. Thompson  
and  
Bernd Ross**

**Approved by**

  
**Robert K. Willardson, General Manager**

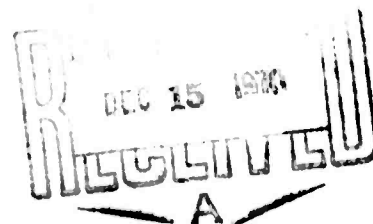
**BELL & HOWELL ELECTRONIC MATERIALS DIVISION  
PASADENA, CALIFORNIA 91109**

**October, 1970**

**Submitted to**

**Office of Naval Research  
Physics Branch  
Arlington, Virginia 22217**

**This document has been approved  
for public release and sale; its  
distribution is unlimited.**



This document has been approved for public release and sale;  
its distribution is unlimited.

Reproduction in whole or in part is permitted for any purpose  
of the United States Government.

This research is part of Project DEFENDER under the joint  
sponsorship of the Advanced Research Projects Agency, the  
Office of Naval Research, and the Department of Defense.

ABSTRACT

The indium arsenide-phosphide alloy system has been studied. Indium arsenide and indium phosphide compounds were prepared by pulling and directional freezing respectively. The InP ingots were characterized for distribution coefficients and electrical properties. Ingots of  $\text{InAs}_{1-x}\text{P}_x$  were pulled by two modifications of the Czochralski technique--an all-quartz sealed system and pulling through a liquid encapsulant. The two methods are compared and the latter found to be superior for these alloys. Electrical, X-ray and mass spectrometric measurements were made on the alloy ingots. Laser diodes were fabricated in a similar manner to those reported on previously, with power outputs up to 0.5W at  $1.06\mu$  with better than 1% efficiency being obtained under pulsed conditions close to 100°K. Amplification of the  $1.06\mu$  emission from an  $\text{InAs}_{1-x}\text{P}_x$  laser diode was demonstrated in a Nd-doped glass fiber, showing a system gain of 50,000.

TABLE OF CONTENTS

	<u>Page</u>
1. INTRODUCTION	1
(a) Statement of Problem	1
(b) Previous Work	1
(c) Summary of Work	2
(d) Acknowledgments	3
2. MATERIAL PREPARATION	4
(a) Preparation of InAs and InP	4
(b) Preparation of InAs <sub>1-x</sub> P <sub>x</sub>	4
3. PHYSICAL PROPERTIES	11
(a) Properties of Indium Phosphide	11
(b) Properties of Indium Arsenide	16
(c) Properties of Indium-Arsenide-Phosphide	16
4. LASER DIODE FABRICATION	24
(a) General Technique	24
(b) Preparation for Diffusion	24
(c) Diffusion	25
(d) Post Diffusion Procedure	27
(e) Ohmic Contacts	34
(f) Fabrication of the Laser Die	34
(g) Laser Die Mounting Procedure	35
5. LASER DIODE EVALUATION	39
(a) Review	39
(b) Electrical and Optical Characterization	41
(c) Spectral Characterization	45
6. OPTICAL AMPLIFICATION EXPERIMENT	49
(a) Diode Selection	49
(b) Glass-Fiber Amplifier Design	49

	<u>Page</u>
6. OPTICAL AMPLIFICATION EXPERIMENT (Con'd)	
(c) Experimental Arrangement	52
(d) Results	56
(e) Conclusions	60
7. CONCLUSIONS	61
8. REFERENCES	64

Form: DD 1473

LIST OF FIGURES

<u>Figure No.</u>		<u>Page</u>
1	Diagram of Apparatus Used for Pulling Crystals by the Sealed Czochralski Technique	5
2	Diagram of Apparatus Used for Pulling Crystals by the Czochralski Technique Under B <sub>2</sub> O <sub>3</sub> Glass	7
3	Carrier Concentration in InP as a Function of Doping Level and Dopant	12
4	Electron Mobility of InP at 300°K as a Function of Carrier Concentration	14
5	Electron Mobility of InP at 77°K as a Function of Carrier Concentration	15
6	Distribution Coefficients in InAs and InP as a Function of Tetrahedral Radius	17
7	Pseudo-binary Phase Diagram for the InAs <sub>1-x</sub> P <sub>x</sub> System	19
8	Distribution Coefficients in InAs <sub>1-x</sub> P <sub>x</sub> as a Function of Alloy Composition	21
9	Schematic Diagram of the Cameca/Bell & Howell Ion Microanalyzer	28
10	Concentration of Zinc in InAs <sub>1-x</sub> P <sub>x</sub> vs. Depth into Slice for Different Diffusion Conditions	31
11	(a) Mounting of Diffused InAsP Material for Polishing	36
	(b) Sketch of Polishing Operation Showing Jig Orientation Relative to Wheel Motion	36
12	Spectral Sensitivity of Silicon Photodiode (type SGD-100) Used to Measure Laser Output Power	38

<u>Figure No.</u>		<u>Page</u>
13	Power Output of $\text{InAs}_{1-x}\text{P}_x$ Diodes as a Function of Carrier Concentration	42
14	Efficiency of $\text{InAs}_{1-x}\text{P}_x$ Diodes as a Function of Carrier Concentration	43
15	Threshold Current Density of $\text{InAs}_{1-x}\text{P}_x$ Laser Diodes as a Function of Carrier Concentration	44
16	Variation of Wavelength of Light Emitted from $\text{InAs}_{1-x}\text{P}_x$ Laser Diodes at 77°K	47
17	Spontaneous Emission Spectral Envelopes for $\text{Nd}^{3+}$ in Various Host Glasses	51
18	Experimental Arrangement for Optical Amplification of Injection Laser Emission	54
19	(a) Light Pulse from $\text{InAs}_{1-x}\text{P}_x$ Injection Laser	57
	(b) Fluorescence from Optical Amplifier	57
20	(a) Optical Amplifier Output 700 $\mu\text{sec}$ After Pump Initiation	58
	(b) Optically Amplified Injection Laser Pulse on Crest of Fluorescence Emission	58

LIST OF TABLES

<u>Table No.</u>		<u>Page</u>
1	Characteristics of $\text{InAs}_{1-x}\text{P}_x$ Ingots Produced by the Liquid Encapsulation Technique	22
2	Diffusion Data for $\text{InAs}_{1-x}\text{P}_x$ Material	26
3	Summary of $\text{InAs}_{1-x}\text{P}_x$ Injection Diode Data	40
4	Properties of Barium-Potassium Silicate Glasses for Laser Use	53

## 1. INTRODUCTION

### (a) Statement of Problem

It has already been shown in work performed under Contract N00014-68-C-0219 that stimulated emission at 1.06 microns can be achieved in  $\text{InAs}_{1-x}\text{P}_x$  diodes. The purpose of this work is threefold.

- (i) Optimization of the  $\text{InAs}_{1-x}\text{P}_x$  injection lasers including associated materials investigations.
- (ii) To study the interaction of  $\text{InAs}_{1-x}\text{P}_x$  stimulated emission with optically pumped Nd-doped YAG or glass laser rods to achieve optical gain.
- (iii) Utilization of the improved  $\text{InAs}_{1-x}\text{P}_x$  injection lasers to demonstrate practical modulated emission from (or amplification in) Nd-doped glass or YAG laser amplifier rods.

### (b) Previous Work

During the course of the previous contract the InAs-InP system was chosen as the most suitable for 1.06 micron injection lasers. Materials studies established a new pseudobinary phase diagram for the system and ingots were grown by the Czochralski technique using two modifications--the sealed-system technique and pulling under  $\text{B}_2\text{O}_3$  glass. InP starting material was generated in a directional freeze apparatus, while the InAs

was pulled in a sealed system. Electrical measurements were made on the InP and  $\text{InAs}_{1-x}\text{P}_x$  boules which, together with mass spectrometric data established distribution coefficients for the major added doping impurities.

Techniques for diffusing, contacting, polishing, cutting and mounting  $\text{InAs}_{1-x}\text{P}_x$  material and devices were developed. Preliminary results showed that lasing was achieved in diodes made from a few of the  $\text{InAs}_{1-x}\text{P}_x$  ingots, with some of the diodes having emission wavelengths of 1.06 microns within experimental error at temperatures close to 77°K. All of this work is fully described in the final report on Contract N00014-68-C-0219, which is reference 1.

### (c) Summary of Work

During the course of the present contract, studies were continued on the InAs-InP system. Section 2 discusses the preparation of the compounds and the alloys, and includes a discussion of the relative merits of the two Czochralski techniques used to prepare  $\text{InAs}_{1-x}\text{P}_x$  boules. Section 3 deals with the physical and electrical properties of the system, and includes the previous work for the sake of completeness. In Section 4 the preparation of laser diodes is discussed, with comments on diffusion in particular which was more fully investigated during the present reporting period. Section 5 gives a summary of the properties of all laser diodes

fabricated under both contracts, including a calibration which was not performed during the first one. Both power and spectral characteristics are reported on. In Section 6 a unique experiment is described. The light emission at  $1.06\mu$  from an  $\text{InAs}_{1-x}\text{P}_x$  laser diode was amplified in a  $\text{Nd}^{3+}$ -doped glass fiber which was optically pumped. A peak gain of 50,000 was realized, demonstrating the feasibility of modulating the high power emission from Nd-doped glass or YAG laser rods by modulating directly a coupled diode laser.

(d) Acknowledgments

This work was under the overall direction of R. K. Willardson, General Manager of the Electronic Materials Division. Dr. A. G. Thompson was chief investigator, with J. W. Wagner directing the materials growth and Dr. B. Ross the device fabrication and evaluation. The able and generous assistance rendered by Dr. E. Snitzer of American Optical Company made possible the diode-laser amplifier experiment, which was performed at the American Optical Company Research Laboratories in Southbridge. We have benefited from discussions with H. Robbins of Bell & Howell Research Laboratories, Drs. R. Behringer and F. Quelle of ONR and Dr. G. Young of American Optical Company. Technical assistance was provided by P. Burke, F. Hicklin, J. W. Nye, K. Schwartz and T. Tench.

## 2. MATERIAL PREPARATION

### (a) Preparation of InAs and InP

The preparation of the compounds in polycrystalline form for making up alloy charges was done in a similar manner to that described in the last reporting period.<sup>1</sup>

The InAs was taken from the polycrystalline portion of boules pulled from undoped melts, and had typical n-type carrier concentrations in the range of  $1 - 5 \times 10^{16} \text{ cm}^{-3}$ .

The InP was prepared by the directional freeze technique described previously.<sup>1</sup> Undoped material having an n-type carrier concentration of less than  $10^{17} \text{ cm}^{-3}$  was usually used as source material, but occasionally doped InP was utilized. In the latter case the amount of dopant was calculated from the amount added in elemental form plus the amount in the compound InP. Some of the better InP was used in the fabrication of laser diodes, while routine electrical measurements yielded useful information [see Section 3(a)].

### (b) Preparation of $\text{InAs}_{1-x}\text{P}_x$

Two different techniques have been used by us to prepare boules of  $\text{InAs}_{1-x}\text{P}_x$ .

The first is a sealed-system in which only quartz and the crucible

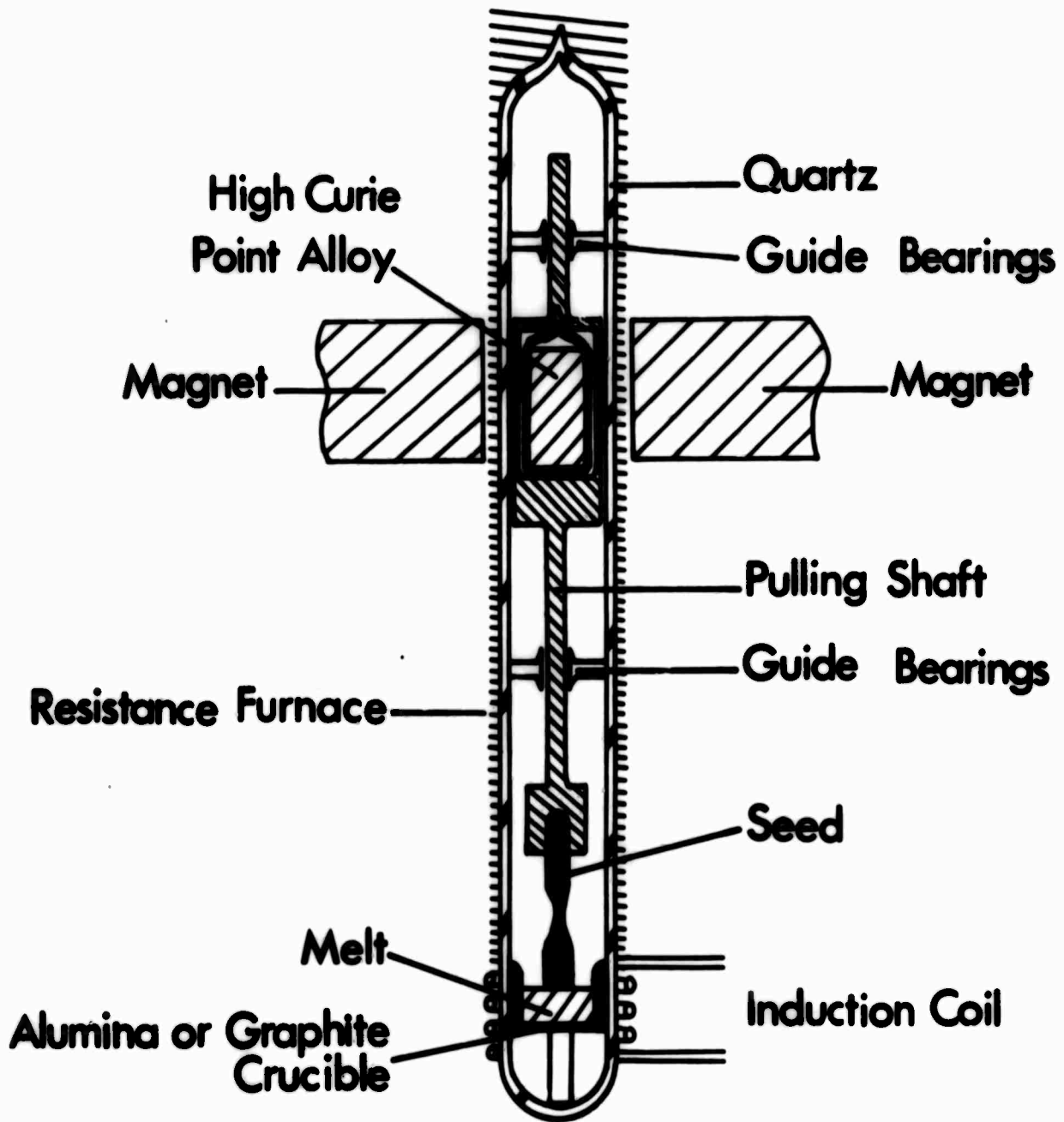


**Figure 1. Diagram of Apparatus Used for Pulling Crystals by the Sealed Czochralski Technique**

material are exposed to the melt and stoichiometry is achieved by controlling the vapor pressure in the chamber. A schematic of the equipment is shown in Figure 1. Vertical motion and rotation are both achieved by magnetic coupling, after a scheme first proposed by Gremmelmaier.<sup>2</sup> The RF heating can either be directly coupled to the melt or to a graphite susceptor surrounding the crucible. In the InAs-InP system it was necessary to pull from non-stoichiometric melts for the phosphorus-rich compositions in order to keep the excess phosphorus/arsenic pressure at 3 atmospheres or less.

The second technique involves direct seed rotation and height control with room temperature seals. The melt overpressure is contained by a blanket of boric oxide ( $B_2O_3$ )<sup>3,4</sup> which has been vacuum-baked in situ to remove all traces of water.<sup>5</sup> An inert gas is used over the  $B_2O_3$  at pressures of 3 atmospheres or less. As with the sealed system non-stoichiometric melts had to be used at the phosphorus-rich end of the system because of the pressure limitations of the puller. The main features of the equipment are shown in Figure 2. RF coupling was to a graphite susceptor containing a fused silica crucible.

Susceptors used with either system were baked out at 1,000°C in vacuo for several hours to minimize contamination. Normal cleanliness precautions were taken with all glassware and the charges. All vacuum pumps and inert

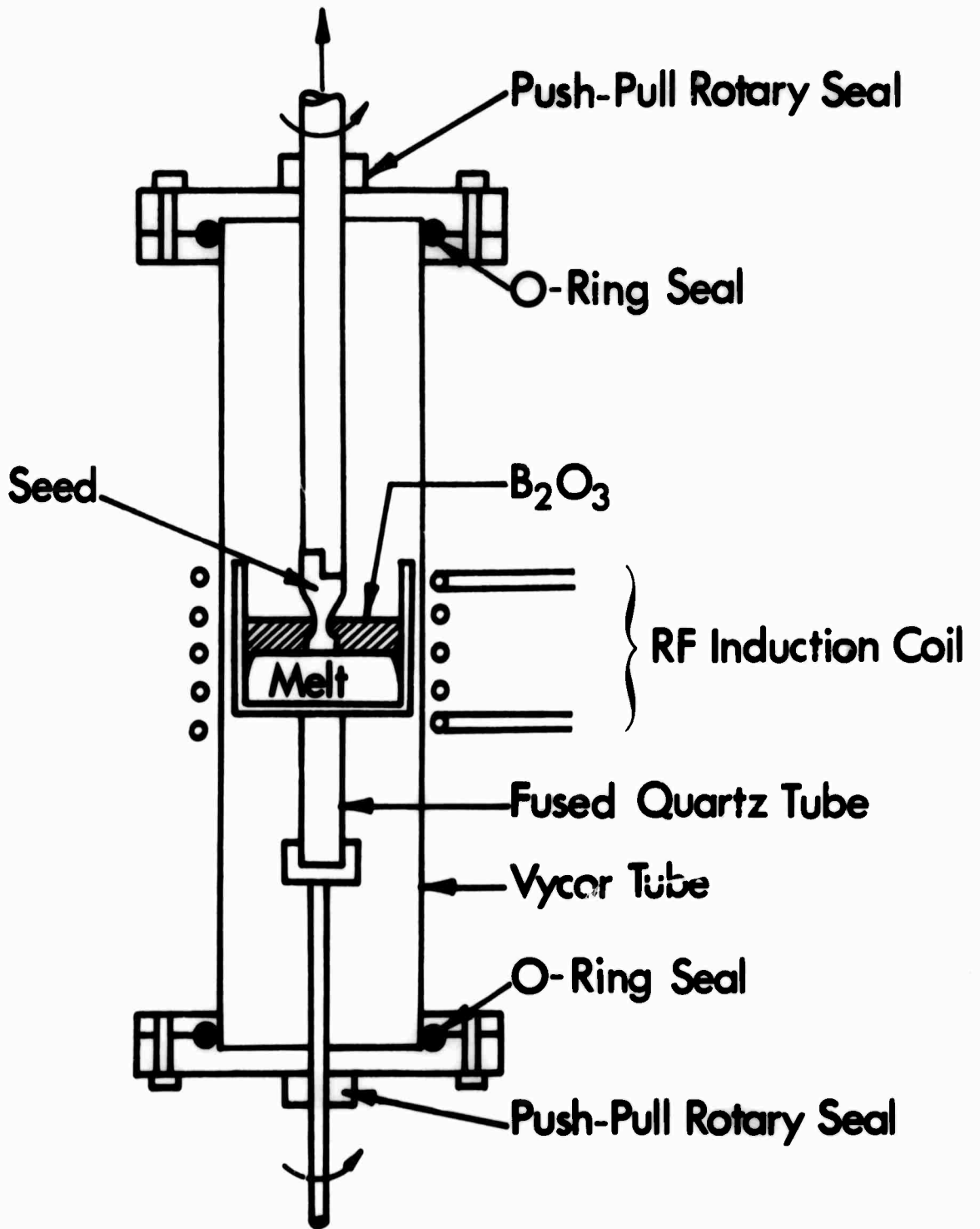


Figure 2. Diagram of Apparatus Used for Pulling Crystals by the Czocharalski Technique Under B<sub>2</sub>O<sub>3</sub> Glass

gases used for flushing or pressurization were trapped with liquid nitrogen.

All of the boules prepared during this contract period were by the second method, that of liquid encapsulation. The reasons for this are discussed below. It was found that precasting the charges led to increased purity and improved visibility through the  $B_2O_3$ . Correct proportions of InP and InAs [see Section 2(a)] and elemental In were weighed out, etched and placed in a fused silica reaction tube. After flushing, a vacuum of  $10^{-4}$  torr or less was pumped and the tube sealed off. The charge was then heated to approximately  $1150^\circ\text{C}$  in a resistance furnace and left at that temperature for two hours under a slow rocking motion. The tube was then rapidly transferred to a bucket of cold water and quenched. The charge was then cleaned (oxides often float to the surface during quenching) and etched, before being used in the puller.

After experience with both systems the liquid encapsulation technique was selected for the following reasons: the pull speed needed for alloys from non-stoichiometric melts is very much smaller than that needed for the compounds. Under these circumstances the poorer mechanical stability of the seed rod in both height and rotation leads to vibrations which may cause the momentary effective pull speed to exceed that necessary for single phase crystal growth. During the previous period many failures

occurred with the sealed system, due to vibrations, excessive pressure and so on. Other advantages of the liquid encapsulation technique include the damping of melt surface vibrations, greatly improved thermal stability across the interface, better radial temperature gradients and simpler puller design and maintenance. Disadvantages are that strain may occur at the growth (liquid-solid) interface due to the presence of the  $B_2O_3$ , impurities floating on the melt cannot volatilize, reacting charges in situ is difficult and usually results in increased impurity levels and decreased visibility and certain dopants such as Si cannot be used since they are gettered by the  $B_2O_3$ . We feel that for many materials, especially those which have to be pulled slowly, the liquid encapsulation technique is superior.

Only polycrystalline boules of  $InAs_{1-x}P_x$  have been prepared to date. It was noticed that as the doping levels were increased the grain size tended to decrease. Since we have been concentrating in the  $10^{19} \text{ cm}^{-3}$  region during this period any improvements have probably been nullified by this effect. It is felt that stoichiometric melts are the best way to achieve single crystal growth, and that a seed development program starting with InP and working out to  $InAs_{0.15}P_{0.85}$  is necessary. This entails pressurizing the melt to 15 to 20 atmospheres for InP, with somewhat less being required for the alloys.

While most of the  $\text{InAs}_{1-x}\text{P}_x$  ingots pulled during this period had  $x \sim 0.85$  (in order to give  $1.06\mu$  emission--see Section 5), ingots prepared during the previous contract and for other projects have been included in most discussions, graphs and data tables in this report for the sake of completeness. Nearly all of these ingots were pulled from non-stoichiometric melts of  $\text{In}_{1-y}(\text{As}_{1-x}\text{P}_x)_y$  where  $y = 0.40 - 0.45$  ( $y = 0.50$  corresponds to a stoichiometric melt).

### 3. PHYSICAL PROPERTIES

#### (a) Properties of Indium Phosphide

The ingots of InP were prepared by a directional freeze technique.<sup>1</sup> Hall bridges were cut from the first-to-freeze ends and from Hall effect and resistivity measurements the carrier concentration, mobility and resistivity were calculated using the simple formulae assuming majority carriers in a single band, i.e.

$$n = \frac{1}{R_H e}, \quad \mu = R_H \sigma$$

It was assumed that all the impurity atoms added as a dopant were electrically active, and this was confirmed for the few cases checked through a mass spectrographic analysis.

The distribution coefficient  $k_0$  was defined<sup>1</sup> as

$$k_0 = \frac{\text{no. of carriers cm}^{-3} \text{ in first part of ingot}}{\text{average no. of impurity atoms cm}^{-3} \text{ in initial melt}}$$

Figure 3 shows the variation of the carrier concentration as a function of the amount of dopant added for sulfur, selenium, tellurium and tin.

Approximate solubility limits of  $3 \times 10^{19} \text{ cm}^{-3}$ ,  $2 \times 10^{19} \text{ cm}^{-3}$  and  $1 \times 10^{19} \text{ cm}^{-3}$  for S, Se and Te respectively were observed. The deviation from a straight line observed for Sn is probably due to the amphoteric nature of this impurity; similar effects have been observed<sup>8</sup> for Si in GaAs

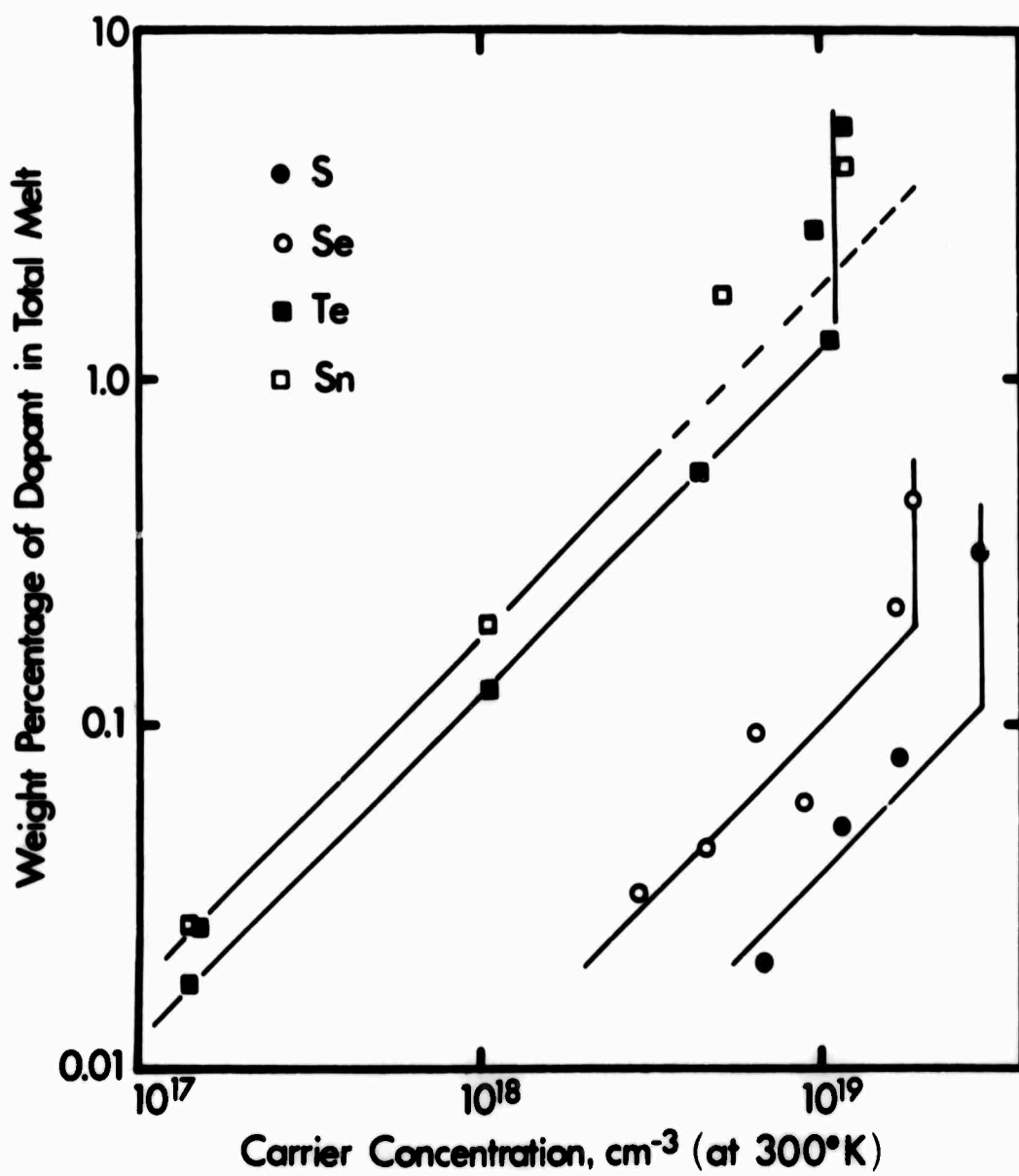


Figure 3. Carrier Concentration in InP as a Function of Doping Level and Dopant

for example. No attempts were made to deliberately dope InP with Si during the course of these programs.

The variation of Hall electron mobility as a function of carrier concentration is shown in Figures 4 and 5 for room temperature and liquid nitrogen temperature respectively. In each case we have plotted our best values along with the best values recorded in the literature.<sup>7,8</sup> It can be seen that the directional freeze material compares favorably with the literature, especially at room temperature. At low temperatures impurity scattering is presumably dominant, and the mobility is therefore quite strongly dependent primarily on the impurity content or carrier concentration. At room temperatures other scattering mechanisms dominate. Both of these have been discussed in detail by Willardson<sup>9</sup> for GaAs, and most of these conclusions apply to InP also.

Since the phosphorus pressure held over the melt in the directional freeze equipment was between 1 and 3 atmospheres a non-stoichiometric growth condition was in effect. This necessitated a slow growth speed and resulted in indium inclusions in the portion of the ingot which was last to freeze. Grain size varied widely, but on average decreased as the carrier concentration increased, especially above  $1 \times 10^{19} \text{ cm}^{-3}$ . The largest grains and highest yield of inclusion-free material were obtained with undoped ingots, the best achieved toward the end of the program being a

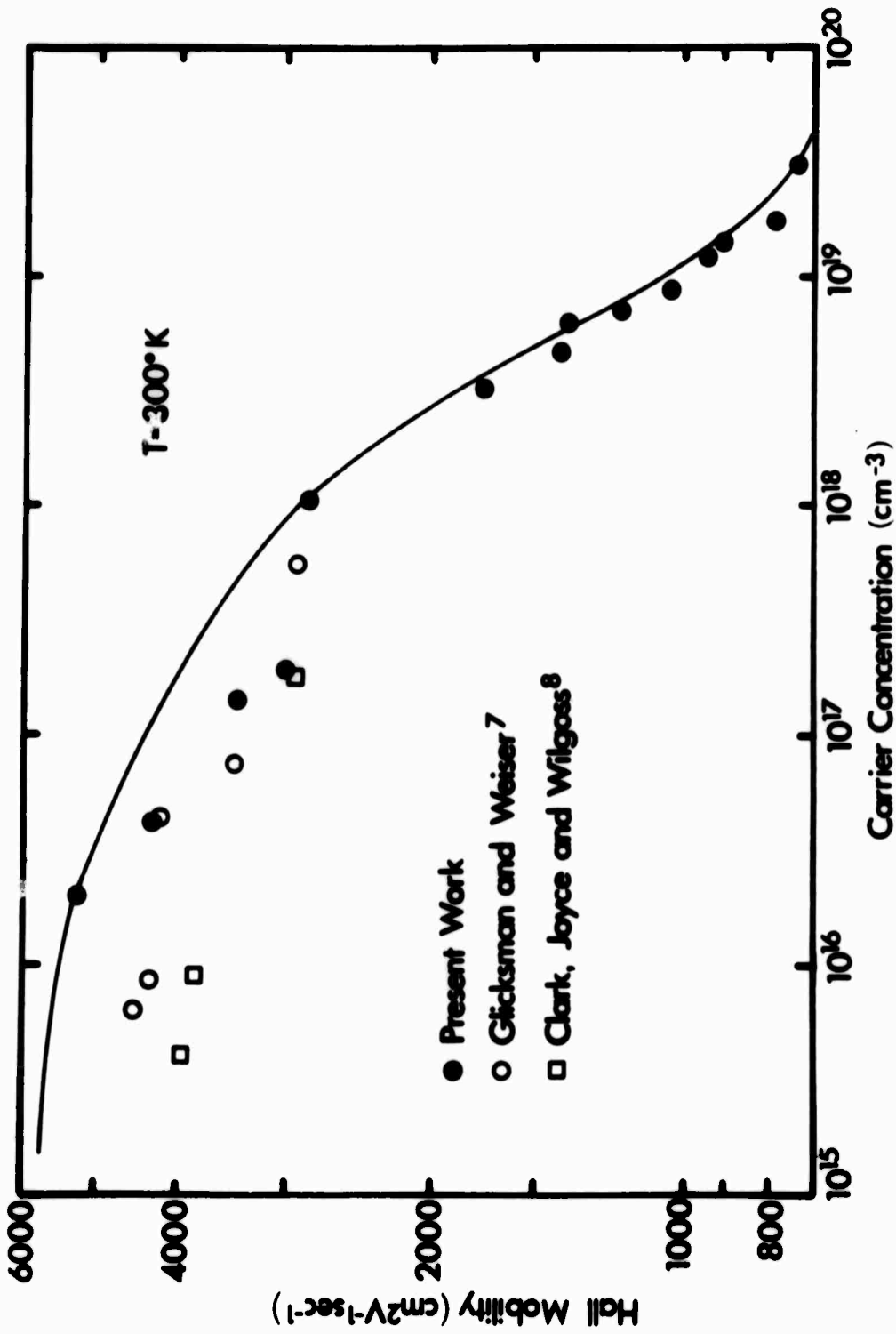


Figure 4. Electron Mobility in InP at 300°K as a Function of Carrier Concentration

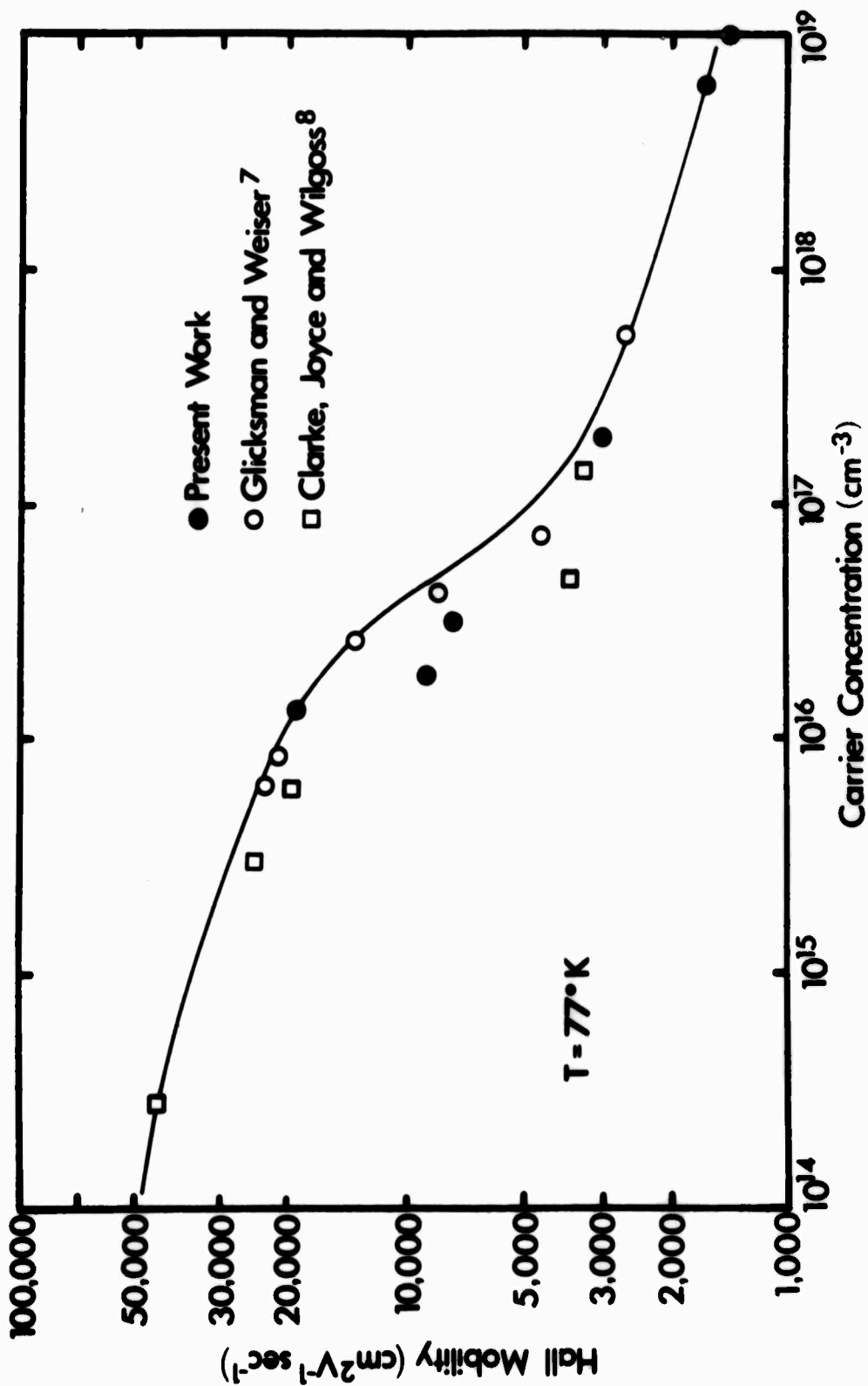


Figure 5. Electron Mobility of InP at 77°K as a Function of Carrier Concentration

single grain approximately  $1 \times 1 \times 3$  cm. Ingots doped in the mid  $10^{18}$   $\text{cm}^{-3}$  range had maximum grain sizes of  $0.2 \times 0.3 \times 1$  cm.

#### (b) Properties of Indium Arsenide

Figure 6 shows the variation of distribution coefficients for some common dopants in InAs and InP as a function of tetrahedral radius. The values for InAs are from the literature<sup>10,11</sup> and our own results in commercial production. Where possible values pertaining to similar growth conditions have been chosen. The values for InP are taken from the present work, described in Section 3(a) above, and some of our unpublished work. It can be seen that the values of  $k_0$  for InP follow a reasonable pattern and are lower than those for InAs. The inversion of the Zn and Sn lines is not thought to be significant.

#### (c) Properties of Indium-Arsenide-Phosphide

The first-to-grow portion of each alloy ingot was analyzed by X-ray powder diffraction techniques. The composition  $x$  was then calculated assuming that the lattice parameter  $a_0$  varies linearly with molecular composition between the end compounds. Values for the latter are well established.<sup>12</sup> This assumption (that Vegard's law applies) is reasonable, since most of the mixed III-V alloys follow it; in particular the  $\text{GaAs}_{1-x}\text{P}_x$  system obeys Vegard's law accurately.<sup>13</sup> The only accurate work<sup>14</sup> published on lattice parameters in the InAs-InP systems actually shows a

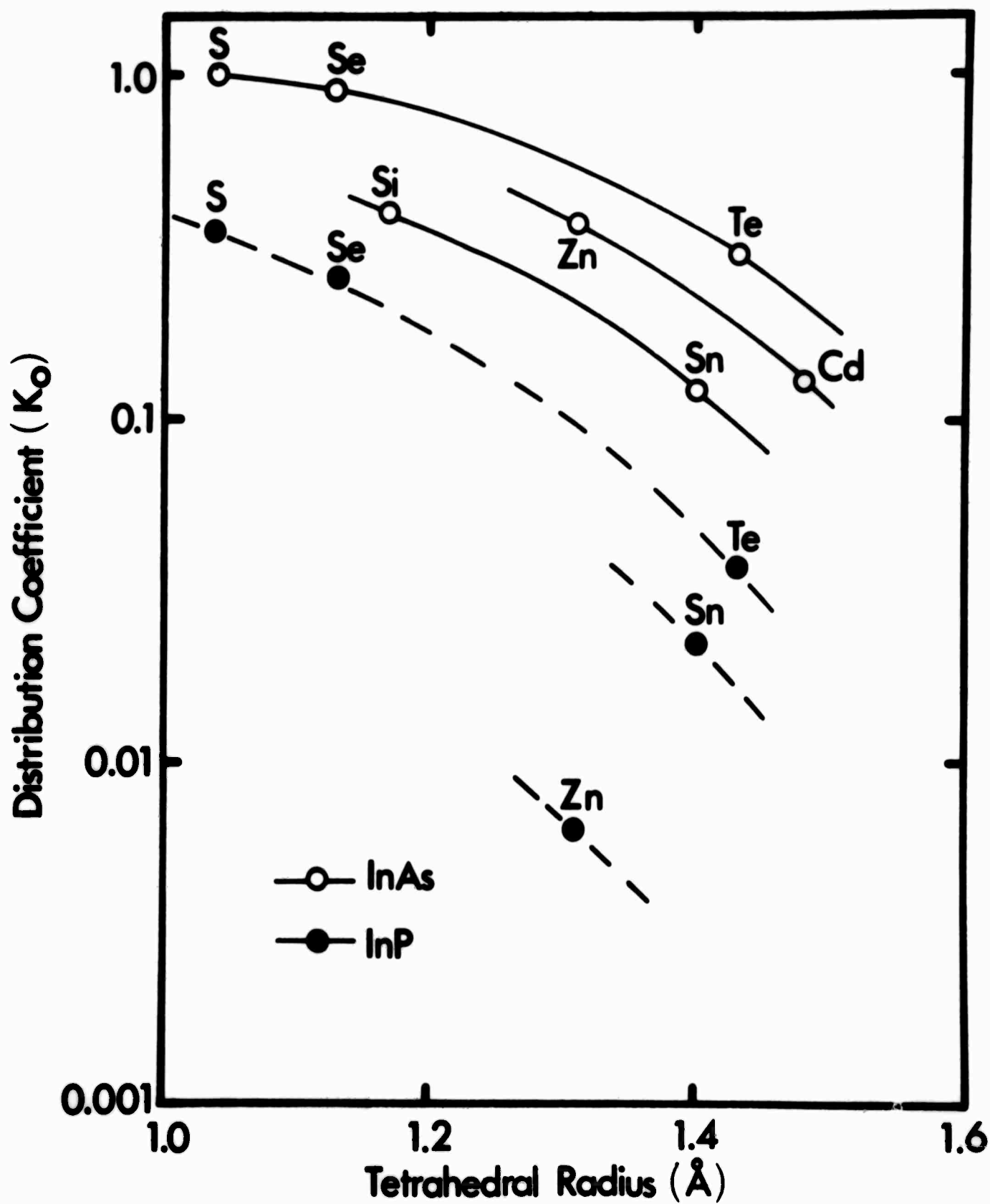


Figure 6. Distribution Coefficients in InAs and InP as a Function of Tetrahedral Radius

slight positive deviation from linearity, but this effect is thought to be due to the method of preparation, and is fully discussed in reference 14.

The purity of the samples and the role of mass spectrographic analysis in determining the composition was discussed at length in the previous report and will not be elaborated on at this time.

A pseudobinary phase diagram has been established in the following manner. The starting composition of the melt was calculated and the composition of the first-to-freeze portion of the ingot (but away from the seed) determined in the manner described above. Since the liquidus-solidus spread is small a symmetrical shape was assumed. This procedure leads to the pseudo-binary phase diagram shown in Figure 7. Also shown are the points obtained by Köster and Ulrich<sup>15</sup>--their much lower liquidus is probably due to the use of inhomogeneous samples which would be expected with their technique. The slight difference between our liquidus and that of reference 15 is probably due to the different pressures and non-stoichiometric conditions used, and it should be stressed that our diagram applies only to alloys prepared in a similar manner to those described in Section 2(b). Recent theoretical work<sup>16</sup> shows the liquidus-solidus separation determined in the course of this program to be reasonable.

The variation of distribution coefficients for certain dopants in

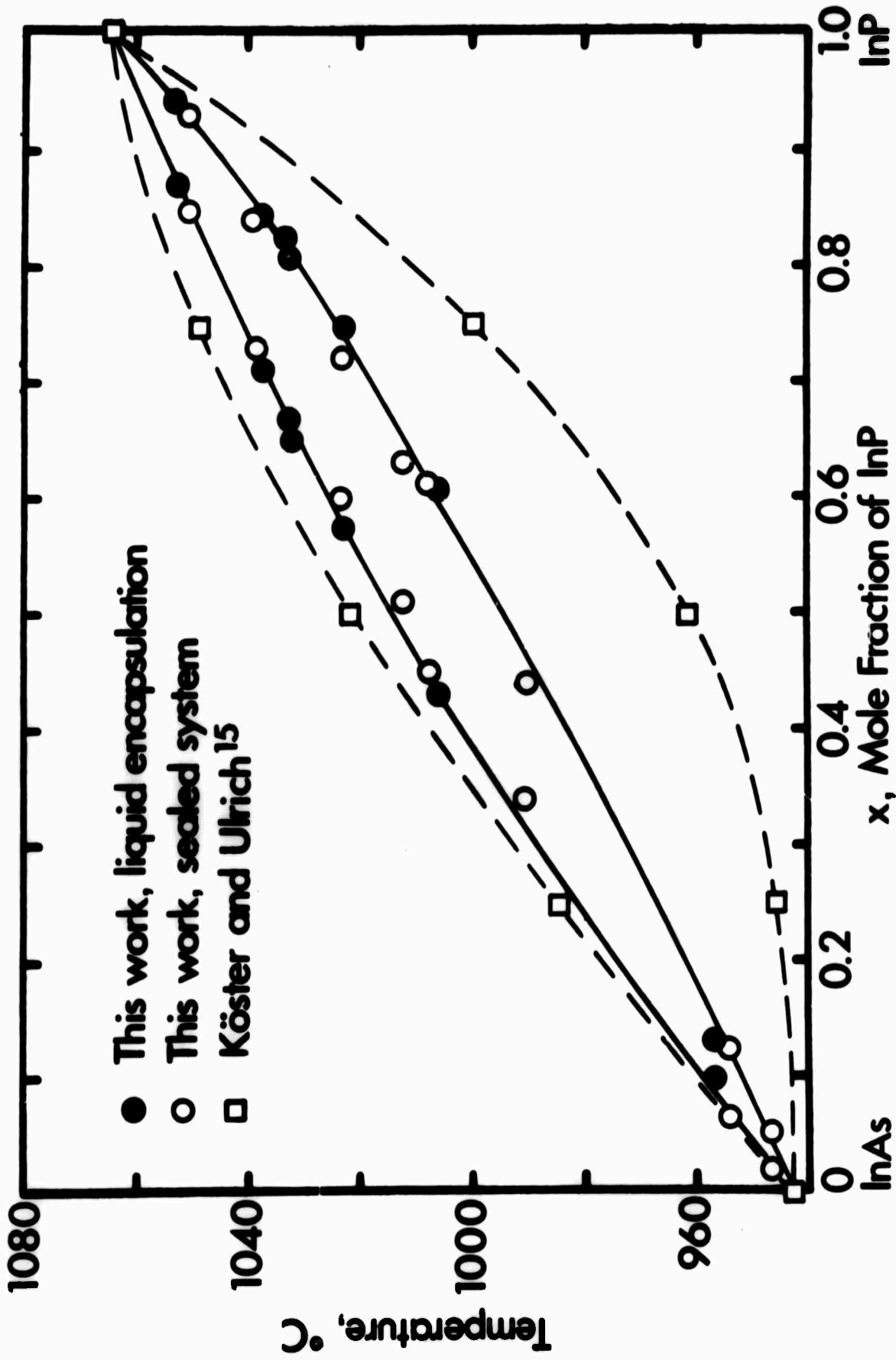


Figure 7. Pseudo-binary Phase Diagram for the  $\text{InAs}_{1-x}\text{P}_x$  System

$\text{InAs}_{1-x}\text{P}_x$  as a function of alloy composition is shown in Figure 8. The behavior is similar to that noted previously,<sup>1</sup> but some values have been checked and new ones added. A notable exception to the general shape of the curves is noted for tin. A possible explanation is that the values for InP and InAs were derived from material prepared under a vapor pressure of the volatile component. The alloys however were grown by the liquid encapsulation technique using boric oxide ( $\text{B}_2\text{O}_3$ ). It has been found in GaAs grown under  $\text{B}_2\text{O}_3$  that silicon (and possibly oxygen) are "gettered" or absorbed by the  $\text{B}_2\text{O}_3$ , which therefore acquires some borosilicate glass. It is possible that tin could act somewhat like silicon but to a lesser extent, permitting some to go into the ingot and some to form a tin oxide which either is absorbed by the  $\text{B}_2\text{O}_3$  or sits between it and the melt surface. Since the tin oxides are usually transparent it is impossible to tell visually that this is happening. It should be noted that the Sn-doped alloys all had  $n \leq 1 \times 10^{18} \text{ cm}^{-3}$  which is well below the limit at which the distribution coefficient begins to vary with concentration [see Section 3(a) and Figure 3].

The properties of the  $\text{InAs}_{1-x}\text{P}_x$  ingots grown during the contract period are summarized in Table 1. The composition was calculated using Vegard's law or taken from the established phase diagram (see above). The carrier concentration, mobility and resistivity measurements were made on bridge-shaped samples in the same way as those made for InP which were described

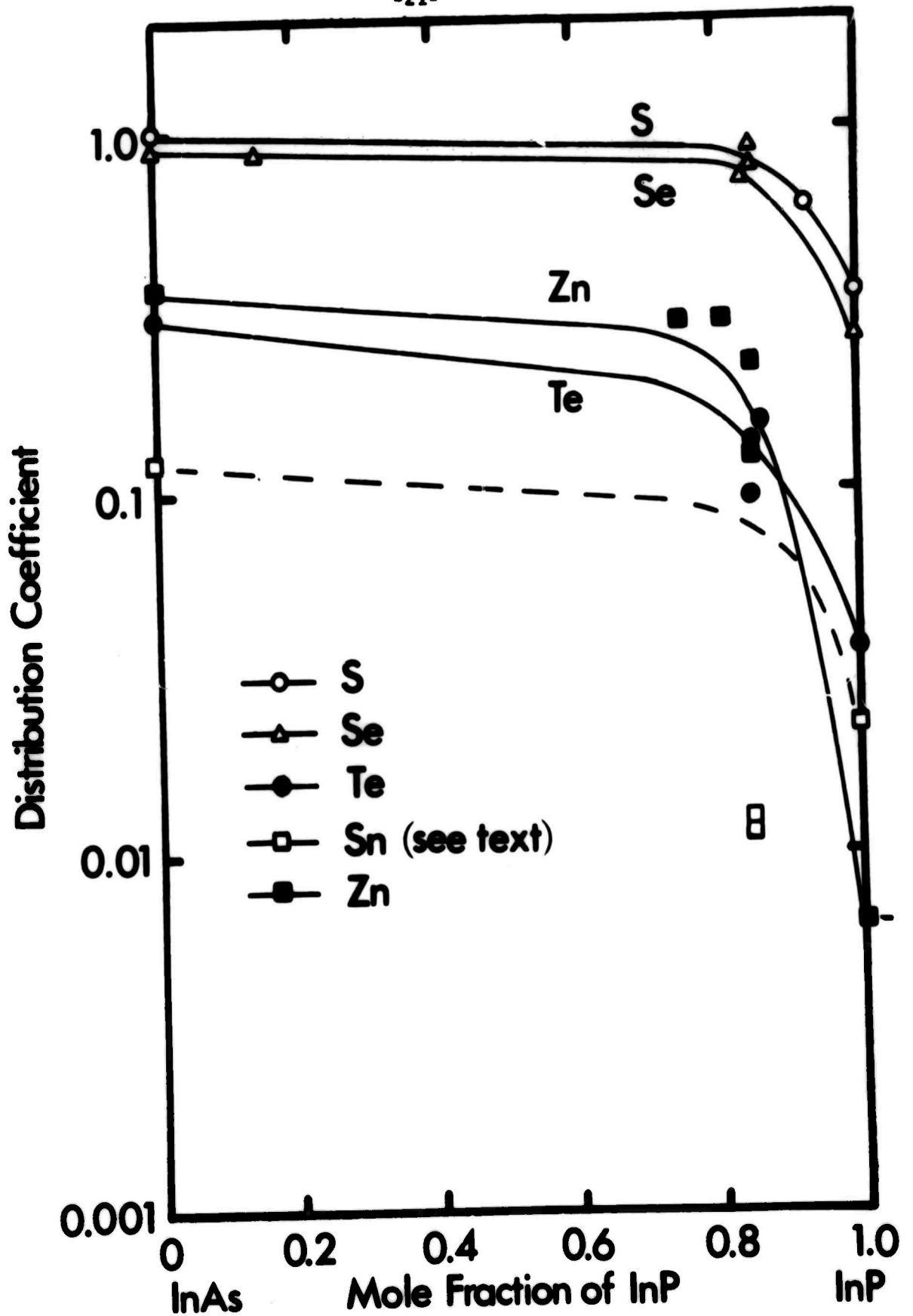


Figure 8. Distribution Coefficients in  $\text{InAs}_{1-x}\text{P}_x$  as a Function of Alloy Composition

TABLE 1

<u>Ingot No.</u>	<u>Dopant</u>	<u>Mol. Fraction InP (x)</u>	<u>No. of Carriers cm<sup>-3</sup></u>	<u>Mobility cm<sup>2</sup>V<sup>-1</sup>sec<sup>-1</sup></u>	<u>Resistivity ohm-cm</u>	<u>Comments</u>
W11	Se	0.845	$3.3 \times 10^{18}$	1900	$1.0 \times 10^{-3}$	
W13	Se	0.130	$4.2 \times 10^{18}$	6800	$2.2 \times 10^{-4}$	
W14	Se	0.845	$1.4 \times 10^{19}$	1300	$3.4 \times 10^{-4}$	*
W16	None	1.00	$2.5 \times 10^{18}$	3950	$6.4 \times 10^{-2}$	
W18	Se	0.845	$4.7 \times 10^{18}$	1600	$8.1 \times 10^{-4}$	*
W19	Se	0.845	$1.2 \times 10^{19}$	1400	$3.7 \times 10^{-4}$	*
W20	Te	0.845	$1.1 \times 10^{19}$	1050	$5.2 \times 10^{-4}$	*
W21	Se	0.845	$1.0 \times 10^{19}$	790	$8.0 \times 10^{-4}$	*
W22	Sn	0.845	$1.3 \times 10^{18}$	2200	$2.2 \times 10^{-3}$	*
W23	Sn	0.845	$6.3 \times 10^{17}$	2150	$4.6 \times 10^{-3}$	
W24	Te	1.00	$9.4 \times 10^{18}$	890	$7.5 \times 10^{-4}$	

Characteristics of  $\text{InAs}_{1-x}\text{P}_x$  alloys produced by the Liquid Encapsulation Technique. All data were taken at room temperature. The values of composition, x, were derived from X-ray powder photographs assuming Vegard's law is valid [see discussion in Section 3(c)].

\* Signifies lasing diodes were fabricated from that ingot. The other ingots were not tried because of poor grain size or lack of time.

in Section 3(a). The comments made previously<sup>1</sup> on the mobility variation in the alloys for undoped samples still apply.

#### 4. LASER DIODE FABRICATION

##### (a) General Technique

In the usual construction of semiconductor injection laser structures made from single crystalline material the fabricator uses the crystalline structure to provide parallelity of the Fabry-Perot cavity reflectors. This is done by taking the single crystal wafer oriented such that  $\langle 110 \rangle$  planes are perpendicular to the surface of the wafer, and cleaving the wafer into strips whose width corresponds to the laser length. Unfortunately such a technique is not usable when dealing with a coarse-grained polycrystalline matrix from which the laser dies are to be fabricated. While it would be feasible to select large grains and X-ray orient them individually, such a task would be most tedious and time-consuming. More conveniently, one may establish a reference surface on the polycrystalline matrix and establish a method of fabrication in which all steps relate to this reference surface. The reference surface establishes the p-n junction plane and the Fabry-Perot surfaces are provided by polishing perpendicular to the reference plane.

##### (b) Preparation for Diffusion

The laser fabrication follows generally the method described in reference 1, although some improvements and simplifications of this method have been incorporated during this contract period. The ingot is examined

in order to obtain clues to determine the optimum directions in which to slice the ingot. This is discussed in some detail in reference 1. The objective was to obtain the largest crystallites possible in the plane of the slice so that a minimum number of grain boundaries is likely to occur within each laser die. Since the crystallites tended to be laminar in the direction of growth this usually resulted in the requirement to cut the ingot along the growth direction. Slices of approximately 0.025 inch thickness were cut and lapped parallel with successively finer abrasives such as No. 1200 and No. 3200 grit. One side of the wafer was polished with Linde C (approximately one micron grit size). This was the reference plane. The wafer was cleaned and dried.

#### (c) Diffusion

The polished wafer was placed in a Vycor capsule along with a quantity of high purity phosphorus adequate to provide approximately one atmosphere of overpressure in a vaporized state, and with a quantity of metallic zinc in the ratio of 4:1 respectively. The diffusion capsule was then evacuated, sealed off and placed in a tube furnace. Diffusions were carried on at temperatures between 750°C and 850°C for times between two and four hours. In recent fabrication processes the diffusion temperature was standardized at 800°C and times were between three and four hours.

TABLE 2

DIFFUSION DATA FOR  $\text{InAs}_{1-x}\text{P}_x$  MATERIAL

Diffusion Source Zn:P (1:4 by weight) in a Closed Ampoule

Ingot No.	Composition Mole Fraction	Carrier		Dopant Type	Temp. °C	Time hrs.	Optical		Comments
		Concentration $n, \text{cm}^{-3}$	Diffusion Depth microns						
N'16	1.00	$6.2 \times 10^{18}$	Se	Se	800	3	25-28	Uniform	
N'19	1.00	$5.1 \times 10^{18}$	Sn	Sn	800	4	28-44		
W14	0.845	$1.4 \times 10^{19}$	Se	Se	800	4	32		
W18	0.845	$4.7 \times 10^{18}$	Se	Se	800	4	70-90	Poor etch, probably non-uniform	
W19	0.845	$1.2 \times 10^{19}$	Se	Se	800	4	60	Uniform	
W20	0.845	$1.1 \times 10^{19}$	Te	Te	800	3	50	Quite uniform	
W21	0.845	$1.0 \times 10^{19}$	Se	Se	800	3	50	Quite uniform	
W22	0.845	$1.3 \times 10^{18}$	Sn	{	800	3	150-180	Irregular, surface alloying Uniform	
		800			3	75			
W23	0.845	$6.3 \times 10^{17}$	Sn	{	800	3	150-180	Irregular	Some areas uniform
					800	3	100-150		

(d) Post Diffusion Procedure

The diffusion capsule was withdrawn from the furnace in such a way as to allow the phosphorus to condense on the capsule wall, at the end furthest from the wafer. Withdrawal rates should be such as to allow wafer cooling at a rate not to exceed 10°C/minute in order to avoid quenching and other deleterious effects. Metallographic sections were taken from the wafer and the diffusion front was visualized by stain etching with concentrated HCl for 10 - 15 seconds. The stain-etched samples were examined under a microscope at 200 - 600 magnification. When the diffusion fronts were planar and the diffusion depths were of suitable magnitude (25 - 60 microns) the wafer was further processed. Minimum diffusion depths of approximately 20 microns were required in order to preclude effects from ohmic contact alloying and penetration to the p-n junction. Typical data concerning diffusions are given in Table 2. In samples W22 and W23 in the Table it appears that anomalous diffusion occurred. This has been discussed in some detail in reference 1. Whether this anomaly resulted from the material properties or from excessive available zinc could not be determined. However, it will be noted that the donor carrier concentration was comparatively low in both cases.

In order to determine the actual zinc concentration profiles in our samples, an ion microanalyzer was used.<sup>17</sup> This machine provides a plasma

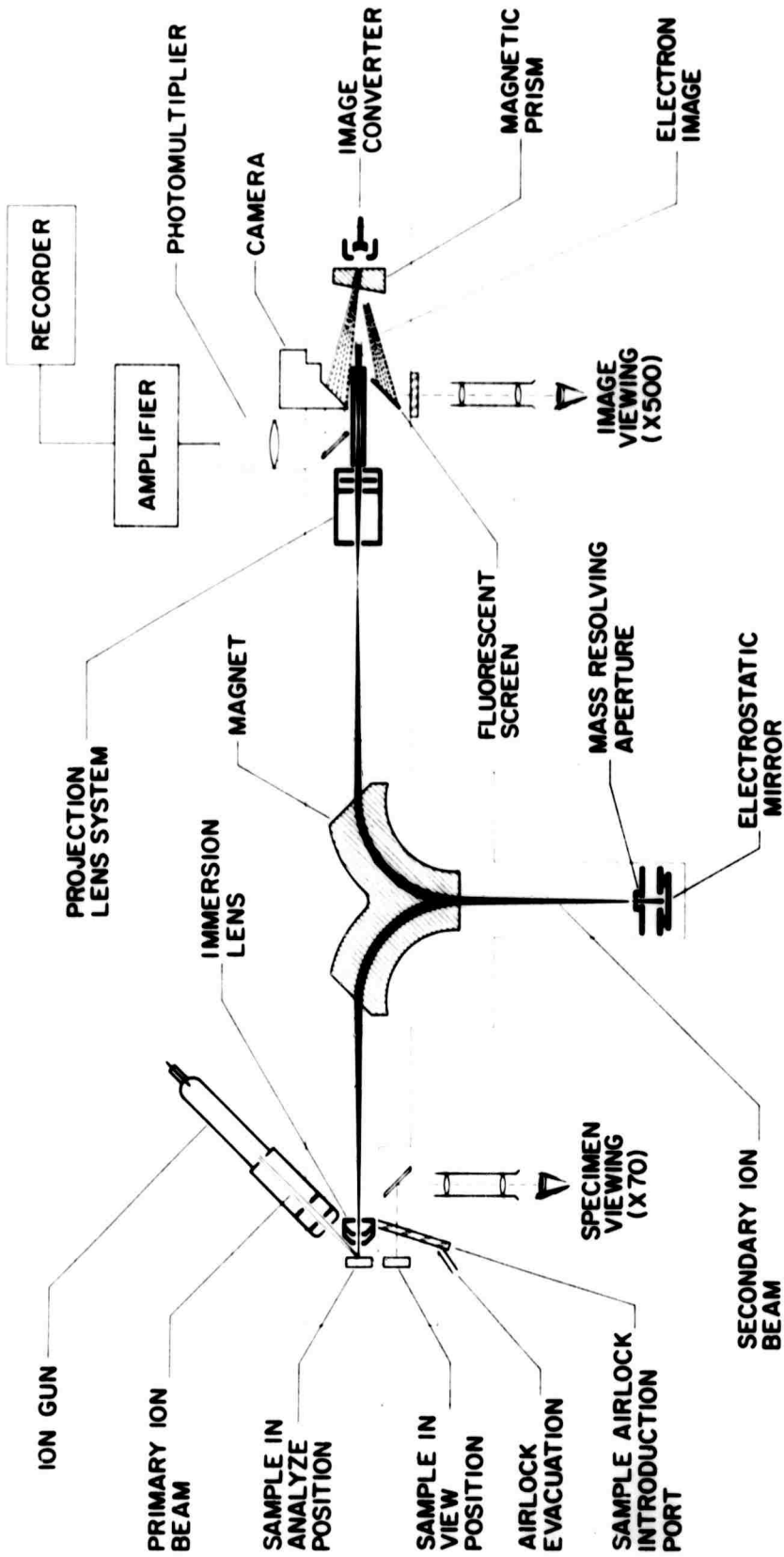


Figure 9. Simplified Diagram of the Ion Microanalyzer

beam of minute cross-section to vaporize a surface spot of the sample. The vaporized atoms are mass spectrographically analyzed and then visualized on a fluorescent screen as a mass-selected image. This apparatus allows viewing of the sample area in order to pre-determine the exact location of the source material, and allows image formation with any of the available source atoms so that the distribution of zinc atoms can be determined in a spatial sense as well as the in-depth quantitative information. This is especially of interest at large impurity concentrations close to the solubility limit where precipitation and aggregate formation may be suspected. A disadvantage of this method is the destruction of the sample in that a depth scan results in a crater from which the material has been sputtered to the desired depth. The operation of the Cameca ion microanalyzer is described in somewhat more detail below.

A simplified schematic view of the Cameca ion microanalyzer used in these experiments is shown in Figure 9. The ion beam emerges from the ion gun on the upper left-hand side and is incident upon the sample on the left side of the diagram. The ionized sputtered material passes through the electrostatic immersion lens, is analyzed and deflected by the magnet to the center of the diagram, and is focused on the mass resolving aperture, through which it passes again after reflection by the electrostatic mirror. The second pass through the analyzing magnet deflects the beam towards the

right side of the page and the electrostatic projection lens images the ions of mass number appropriate to the aperture setting upon the image converter. The image can be analyzed by the options shown in the diagram: (1) direct viewing on the fluorescent screen; (2) obtaining a photograph with the camera; (3) obtaining a quantitative measurement with a photomultiplier operating into a recorder. The mass resolution of the arrangement is approximately 300. The depth resolution is  $50\text{\AA} - 100\text{\AA}$  and the spatial resolution is about one micron.

Figure 10 depicts the zinc concentration profiles of three samples diffused at different times and temperatures. The top curve shows the diffusion profile of zinc diffusion at  $900^{\circ}\text{C}$  at one hour. It appears that the surface concentration is approximately  $1 \times 10^{20}$  atoms  $\text{cm}^{-3}$ . For this sample the junction occurs at approximately 65 microns from the surface (at the point where the zinc concentration equals the sulfur concentration of  $1.6 \times 10^{19}$  atoms  $\text{cm}^{-3}$ ). The second curve from the top gives the data on a sample diffused at  $800^{\circ}\text{C}$  for three hours with a surface concentration of approximately  $2.5 \times 10^{19}$  atoms  $\text{cm}^{-3}$ . The curve appears to be linear but with two distinct slopes which may be the effect of lowering the activation energy during the initial anomalous diffusion for the first 20 - 30 microns of the curve. In this case the junction occurs at approximately 30 microns. The lowest curve results from a sample diffused at  $700^{\circ}\text{C}$  for

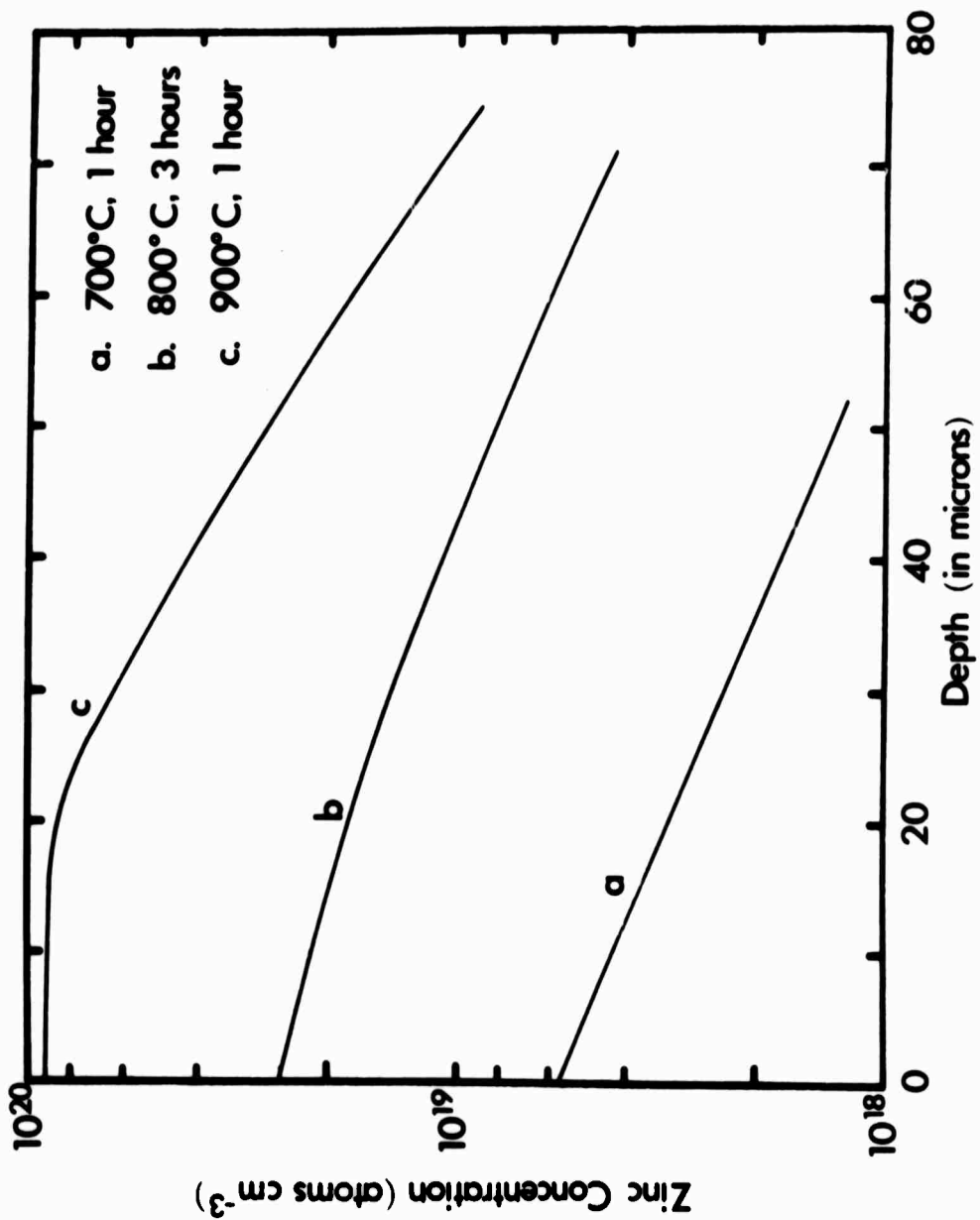


Figure 10. Concentration of Zinc in InAs<sub>1-x</sub>P<sub>x</sub> vs. Depth into Slice for Different Diffusion Conditions

one hour. The surface concentration is  $5.5 \times 10^{18}$  atoms  $\text{cm}^{-3}$  and it is evident that no junction could occur in this sample.

With regard to the ion microanalyzer experiment it must be stated that the first few atomic layers (approximately  $50\text{\AA}$ ) cannot be measured quantitatively due to the interference of adsorbed chemical species and the presence of oxygen which results in a very high initial sputtering yield and subsequent amplifier excursion. The ion beam must therefore be blanked off initially in order to preclude saturating the electronics for significant time intervals.

From the early results<sup>1</sup> it appeared that the diffusion depth is proportional to the square root of time and follows the relation

$$D = D_0 \exp \left( \frac{-E_A}{kT} \right)$$

where  $D$  is the diffusion coefficient,  $D_0 = 10^{-4} \text{cm}^2 \text{sec}^{-1}$ ,  $E_A$  is the activation energy and  $= 1.5 \text{ eV}$ ,  $k$  is Boltzmann's constant and  $T$  is the absolute temperature. It should be stressed that these data were not very extensive and a rather small temperature interval was used. However, the values of  $D_0$  and  $E_A$  are reasonable when compared with the literature (see reference 1 and discussion therein). Most of the results were taken at a temperature of  $800^\circ\text{C}$  and resulted in typical diffusion constants ( $D$ ) of  $1$  to  $2 \times 10^{-9} \text{cm}^2 \text{sec}^{-1}$  for both  $\text{InP}$  and  $\text{InAs}_{0.15}\text{P}_{0.85}$ , with the compound value probably

being smaller than that of the alloy.

Surface concentrations were obtained with the ion microanalyzer (see e.g. Figure 10) and Fick's laws were assumed to hold. At very high surface concentrations and/or low phosphorus overpressures, the diffusion "constant" becomes a function of the zinc concentration (anomalous diffusion) and Fick's laws are no longer obeyed. These conditions were avoided in our experiments (see Section V, in reference 1).

Data in the literature concerning the diffusion of zinc in  $\text{InAs}_{1-x}\text{P}_x$  concerning the diffusion of zinc in  $\text{InAs}_{1-x}\text{P}_x$  or InP are not extensive. Arseni, Boltaks and Dzhaferov<sup>18</sup> studied the diffusion of radioactive Zn in InP and the InAs-rich alloys, using elemental Zn and powdered compound in the closed ampoule. They obtained a diffusion coefficient at 800°C of  $1 \times 10^{-7} \text{ cm}^2 \text{ sec}^{-1}$  for  $x = 0.5$  and  $4 \times 10^{-8} \text{ cm}^2 \text{ sec}^{-1}$  for  $x = 1.0$  (InP). Their concentration vs. depth curves have a similar form to ours (see Figure 10 and text above), but because of their diffusion method and use of highly doped (Zn) samples we have not attempted a direct comparison. Chang and Casey<sup>19</sup> studied the diffusion of radioactive Zn in InP using only an elemental source. Once again, profiles were obtained but comparison is difficult. Their diffusion coefficient at 800°C ranged from  $10^{-8}$  to  $10^{-9} \text{ cm}^2 \text{ sec}^{-1}$ , being concentration dependent (see reference 19 and discussion in reference 1). Comparison of surface concentrations shows good agreement

with Arseni et al<sup>18</sup>, but our results are lower than those of reference 19 by approximately an order of magnitude for the same temperatures. The different methods of diffusion are probably responsible for this.

Prior to the mass spectrometric ion analyzer experiment, attempts were made to measure surface concentration by means of differential capacitance measurements on Schottky barrier diodes. A number of trials were made using evaporated gold contacts. However, in every case the resulting current-voltage characteristics were linear and in no case could a barrier be found.

#### (e) Ohmic Contacts

After diffusion the surface opposite the reference plane was carefully lapped with No. 1200 grit and finished with No. 3200 grit in order to provide a thickness of 0.005 - 0.007 inch. Since alloy semiconductor wafers of this thickness are quite fragile, great care must be used in subsequent handling. The gold-indium-tin contacts on the n-side and gold-indium-zinc contacts on the p-side were prepared by evaporation on the hot substrate similar to the method described in reference 1. I-V measurements indicated typical series resistances on the order of 0.5 ohms for the mounted diodes.

#### (f) Fabrication of the Laser Die

A glass slide (microscope) was prepared to have a thickness equal to

the desired laser cavity length, which in our case was normally 10 - 15 mils. A strip of the diffused wafer was mounted parallel to the cut edge of the glass slide, so that the reference plane of the semiconductor wafer was perpendicular to the prepared glass slide. This was done with jiggging shown in Figure 11a. This figure shows a hot plate next to a surface block supporting a spacer on which the semiconductor wafer rests. A precision rectangular block with sides forming exact 90° angles was used to support the glass slide by means of an elastic band. Red sealing wax was used to mount the semiconductor wafer strip against the glass slide. Excess semiconductor material was then trimmed away from the glass slide by means of a wire saw. The exposed semiconductor strip edge was then ground and polished with successively finer grit sizes such as No. 3200, Linde C, and Linde A. The tendency of the strip of semiconductor material to detach from the glass slice polishing jig was suppressed by assuring that the direction of wheel rotation was into the semiconductor surface and then toward the glass. This is also shown in Figure 11b. After both sides of the semiconductor strip were polished, the polished strip was remounted on another glass slide and wire-sawed into laser dies of appropriate width (5 - 7 mils).

#### (g) Laser Die Mounting Procedure

The laser die mounting procedure described in reference 1 was retained without change. This consisted of mounting the die surrounded by a semi-

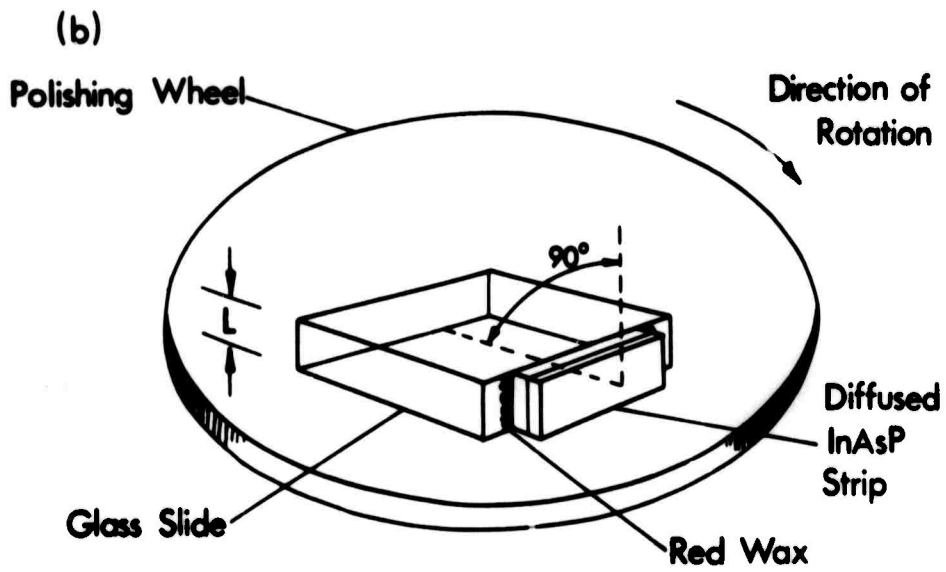
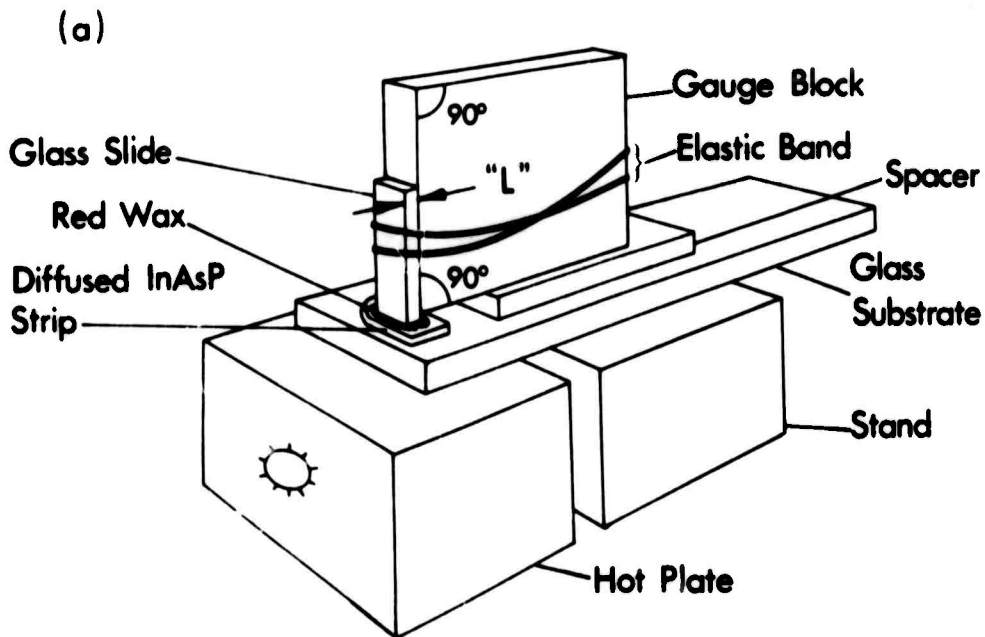
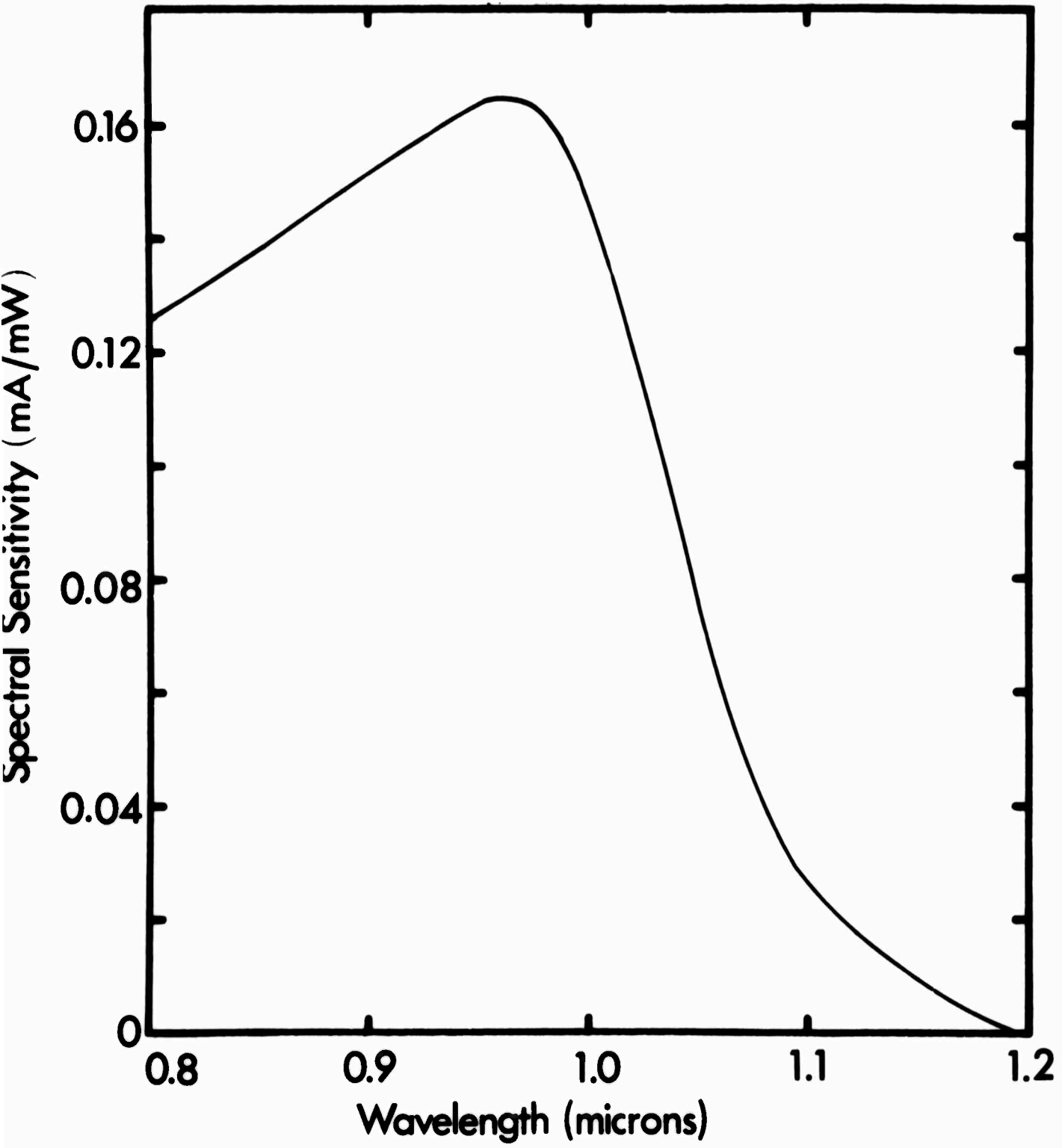


Figure 11a. Mounting of Diffused InAsP Material for Polishing

Figure 11b. Sketch of Polishing Operation Showing Jig Orientation Relative to Wheel Motion

insulating GaAs spacer approximately 1/2 - 1 mil thinner than the laser die, between two indium-coated copper strips. This procedure allowed good contacting of the ohmic electrodes without subjecting the laser die to additional heat treatments or undue stress.



**Figure 12. Spectral Sensitivity of Silicon Photodiode (type SGD-100) Used to Measure Laser Output Power**

## 5. LASER DIODE EVALUATION

### (a) Review

In order to arrive at the objective of this contract, namely the fabrication of efficient lasers operating at 1.06 microns, a variety of materials with varying bandgaps, crystallinity, different electrical properties and various configurations were produced and evaluated. The wealth of properties resulting were difficult to correlate to the systematic variation of parameters, especially in view of the arbitrary crystallinity of the polycrystalline matrices.

Without doubt, some of the variations in the data resulted from grain boundaries within the volume of the device, which may have led to p-n junctions within a laser not lying in a single geometric plane, and possible discrete jumps in composition. Such defects may explain such phenomena as discrete spatial structure of the laser beam suggestive of double source interference and lasing at subsidiary discrete wavelengths respectively, both of which were observed in reference 1, pp. 73 and 87. Scatter in output power, efficiency and threshold data is also evident. This originally led us to believe that the optimized laser structure will be fabricated from material with doping close to the solubility limit. It does appear that the optimum carrier concentration for InAsP laser diodes is considerably higher than that in the case of GaAs laser diodes<sup>20</sup> ( $\sim 2 \times 10^{18} \text{ cm}^{-3}$ ).

TABLE 3

DATA ON  $\text{InAs}_{1-x}\text{P}_x$  INJECTION LASER DIODES

All lasing data were taken at approximately 110°K, except for\* which were taken at 80°K. Values from previous work are included since these have been extended and corrected in some cases. \*\* - did not lase.

Ingot No.	Composition Mole Fraction	Carrier Conc. at 300°K $\text{cm}^{-3}$	Dopant	Max. Output Power $\text{mW}$	Min. Threshold Current $\text{KA cm}^{-2}$	Mean Output Wavelength at $\sim 110^\circ\text{K}$ , $\mu\text{microns}$
N'16	1.00	$6.2 \times 10^{18}$	Se	1.0	-**	0.923
N'19	1.00	$5.1 \times 10^{18}$	Sn	100	4.4	0.914
W6	0.945	$4.0 \times 10^{16}$	None	35	-**	0.958
H22*	0.93	$1.6 \times 10^{19}$	S	90	2.1	0.980*
H23	0.86	$6.7 \times 10^{18}$	Se	350	3.9	1.056
H18	0.855	$1.5 \times 10^{19}$	Te	480	3.7	1.024
W14	0.845	$1.4 \times 10^{19}$	Se	250	4.3	1.040
W18	0.845	$4.7 \times 10^{18}$	Se	220	6.3	1.051
W19	0.845	$1.2 \times 10^{19}$	Se	160	3.7	1.061
W20	0.845	$1.1 \times 10^{19}$	Te	80	6.3	1.043
W21	0.845	$1.0 \times 10^{19}$	Se	180	14	1.045
W22	0.845	$1.3 \times 10^{18}$	Sn	350	4.2	1.052
H21	0.835	$1.9 \times 10^{18}$	Te	280	3.9	1.064
W8	0.825	$2.5 \times 10^{18}$	Se	110	8.4	1.072

(b) Electrical and Optical Characterization

As previously,<sup>1</sup> diodes were first characterized to determine lasing by observing non-linearity of the optical output as a function of current input. A total of 70 devices was characterized, and of these all but 7 exhibited lasing. This number includes 6 from one ingot which was undoped (W6) and had a carrier concentration of only  $4 \times 10^{16}$  electrons  $\text{cm}^{-3}$ ; the optical output of devices made from this crystal was quite respectable (up to 36 mW). As can be seen in the summary of laser output data in Table 3, the maximum power obtained was almost 0.5 watt peak. The minimum threshold current density was from  $2 - 3 \times 10^3$  A  $\text{cm}^{-2}$  and the peak efficiency was approximately 2% at 100°K. Diodes were pulsed at low rep rates of approximately 100 Hertz with an SCR capacitor discharge pulser described previously.<sup>1</sup> The pulse had a triangular shape with a width at half maximum amplitude of approximately 180 nanoseconds. A silicon photodiode (type SGD-100, Edgerton, Germeshausen and Grier) was used as the sensor. The spectral sensitivity of this device is shown in Figure 12, and is typical of silicon devices. This was obtained by comparison to a calibrated standard solar cell (Centralab) with a calibration traceable to the National Bureau of Standards. The efficiency and power measurements were calculated using these absolute spectral response curves.

Figure 13 shows power outputs of different diodes plotted against carrier concentration. Both maximum and mean power outputs are given in

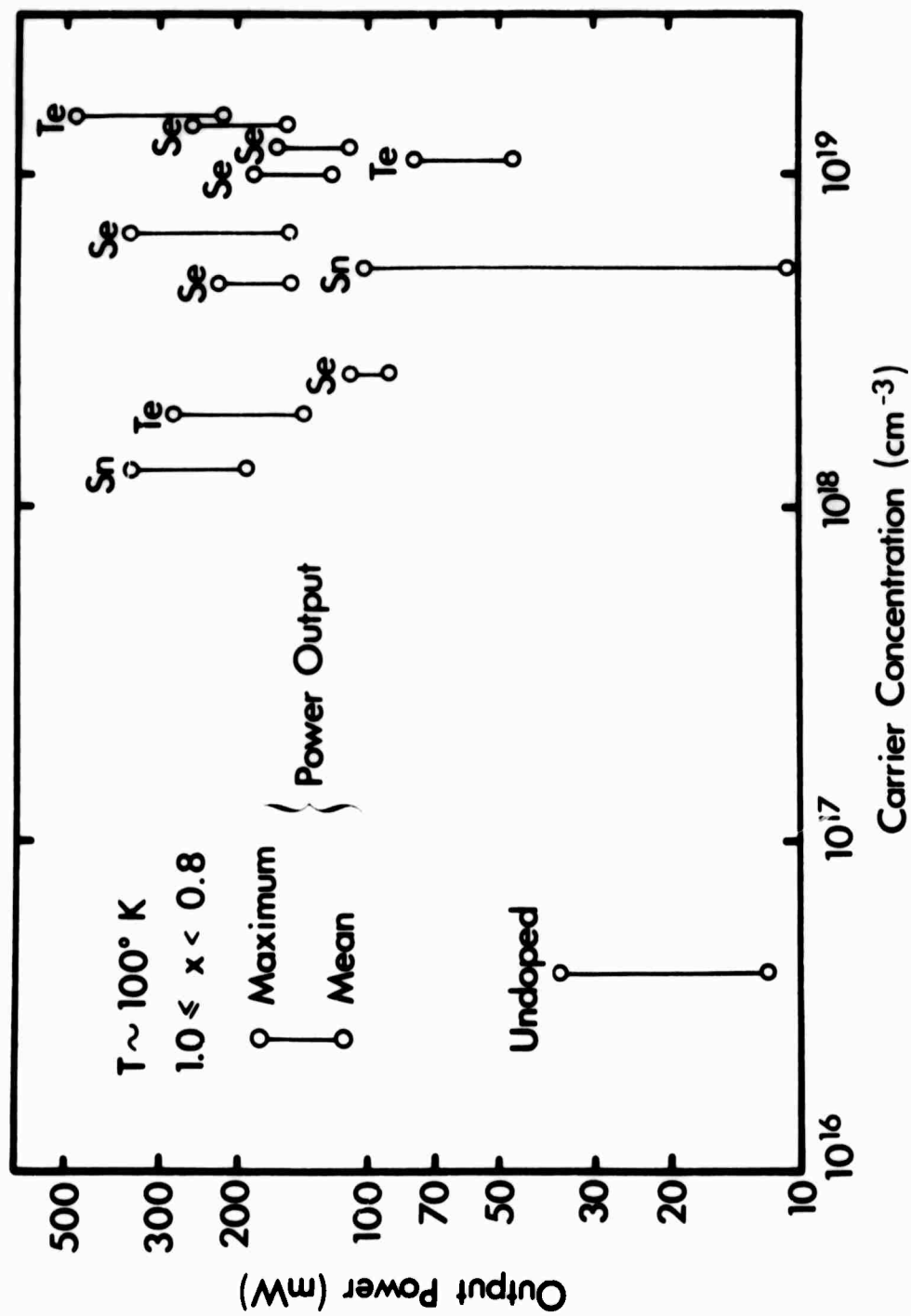


Figure 13. Power Output of  $\text{InAs}_{1-x}\text{P}_x$  Diodes as a Function of Carrier Concentration

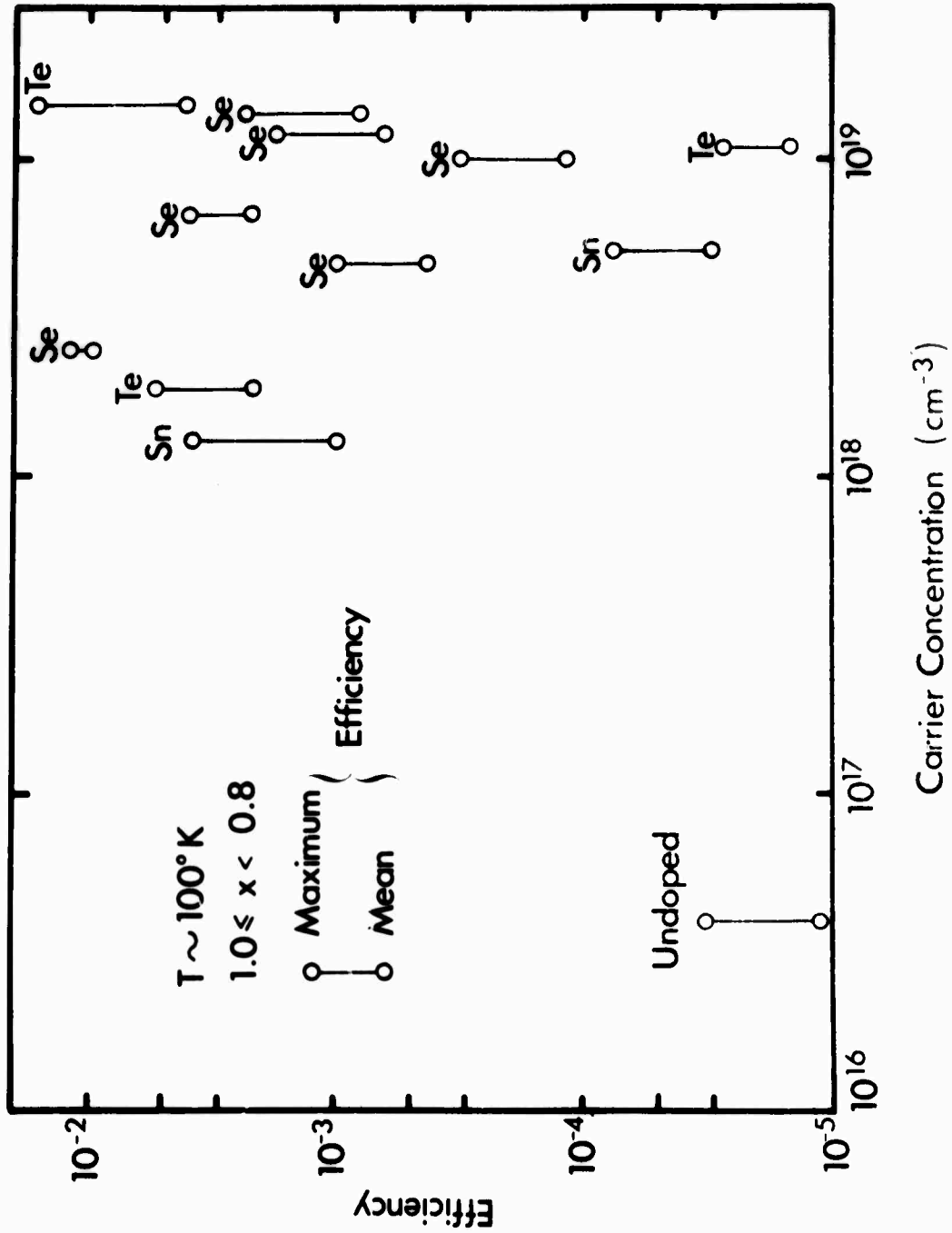


Figure 14. Efficiency of  $\text{inAs}_{1-x}\text{P}_x$  Diodes as a Function of Carrier Concentration

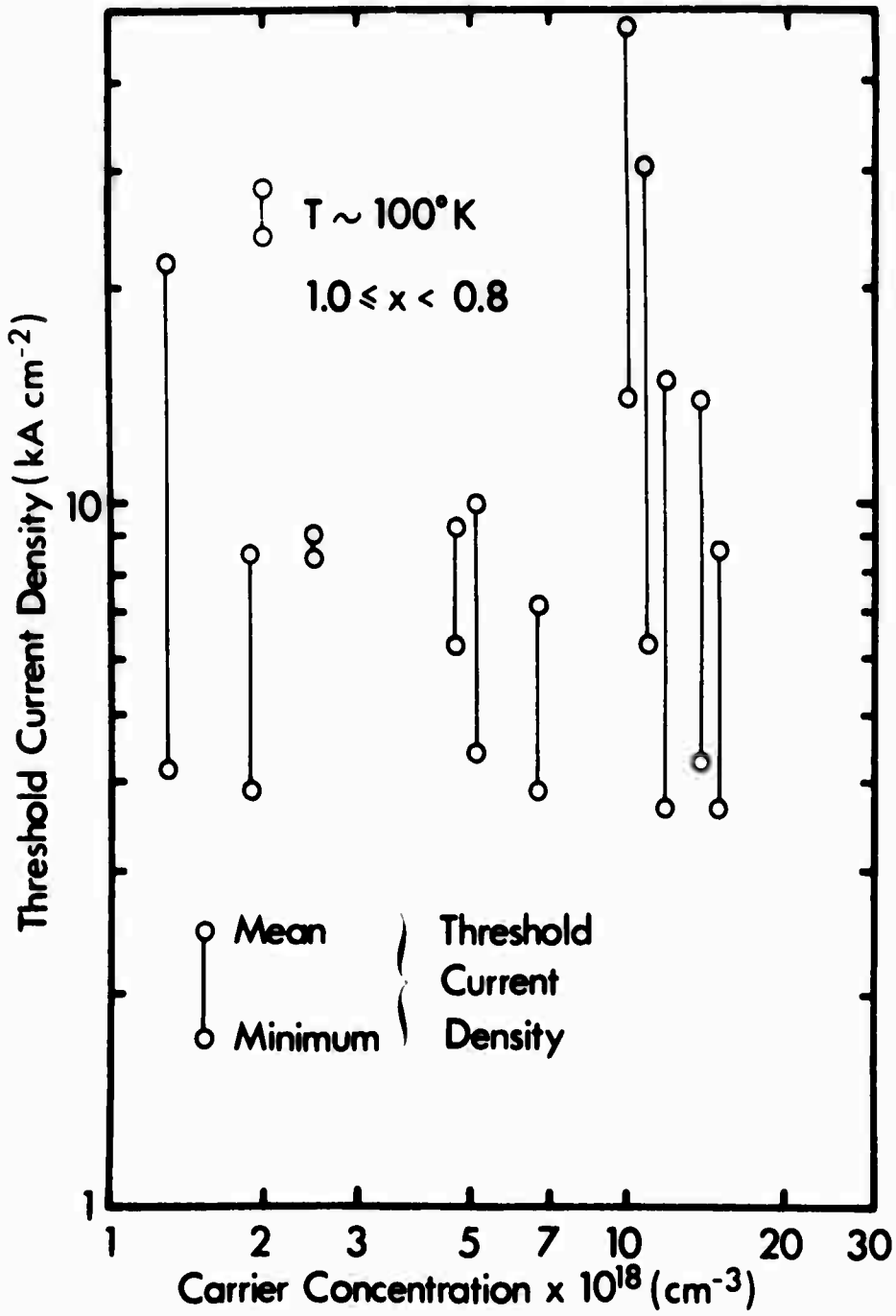


Figure 15. Threshold Current Density of InAs<sub>1-x</sub>P<sub>x</sub> Laser Diodes as a Function of Carrier Concentration

milliwatts with doping species included above each laser group. The grouping does not appear to favor any particular impurity, but the Group 6 shallow donors, S, Se, and Te appear to give the best results. The graph also bears out the contention that high carrier concentrations are beneficial from the standpoint of power output. In Figure 14 the efficiency of diodes is given as a function of carrier concentration. The variation between maximum and mean efficiencies is reasonably narrow and again the high carrier concentrations are favored. Figure 15 gives the threshold current densities as a function of carrier concentrations, indicating both mean and minimum threshold current densities. It is evident that the minimum threshold current density for this group of diodes is independent of carrier concentration, although the grouping again appears to favor concentrations of the order of  $1.5 \times 10^{19} \text{ cm}^{-3}$ .

#### (c) Spectral Characterization

Spectral data generated from later groups of diodes are similar to those previously published,<sup>1</sup> which for the sake of brevity are not reproduced here. Similarly, beam width and spectral line width data follow those in the report of reference 1. Some points were obtained by immersing the laser diodes in liquid nitrogen; these show distinctly lower thresholds which can be attributed to the significantly lower temperature. This temperature was verified by observing the spectral shift of the output emission.

The spectral shift of both coherent and spontaneous emission for devices made of  $\text{InAs}_{0.17}\text{P}_{0.83}$  was observed as a function of temperature. Temperature was measured by means of a thermocouple inserted into the stripline laser holder and by using constant temperature solid-liquid mixtures such as ethylene bromide (154°K). The highest temperature at which coherent outputs could be obtained was 140°K. The measured spontaneous shift gave

$$\frac{d\lambda}{dT} = 1.6 \text{ \AA}/^{\circ}\text{K}$$

resulting in temperature dependence of the energy gap of

$$\frac{dE_g}{dT} = -1.8 \times 10^{-4} \frac{\text{eV}}{^{\circ}\text{K}}$$

Figure 16 gives the spectral variation of emitted light vs. composition between pure InP and 80% InP. The points are the arithmetic mean of the maximum spread of values of laser diodes taken from any one ingot. All data were corrected to 77°K using the measured temperature coefficients. The curve was least-squares fitted to all x-values obtained by us (reference 1 and present work) and those points available from the literature<sup>21-24</sup> to a parabola, after the suggestion of Thompson and Woolley.<sup>25</sup> A good fit was obtained for the  $\text{InAs}_{1-x}\text{P}_x$  laser diodes using the relation

$$E_{\gamma\gamma}(\text{eV}) = 0.395 + 0.747 x + 0.224 x^2$$

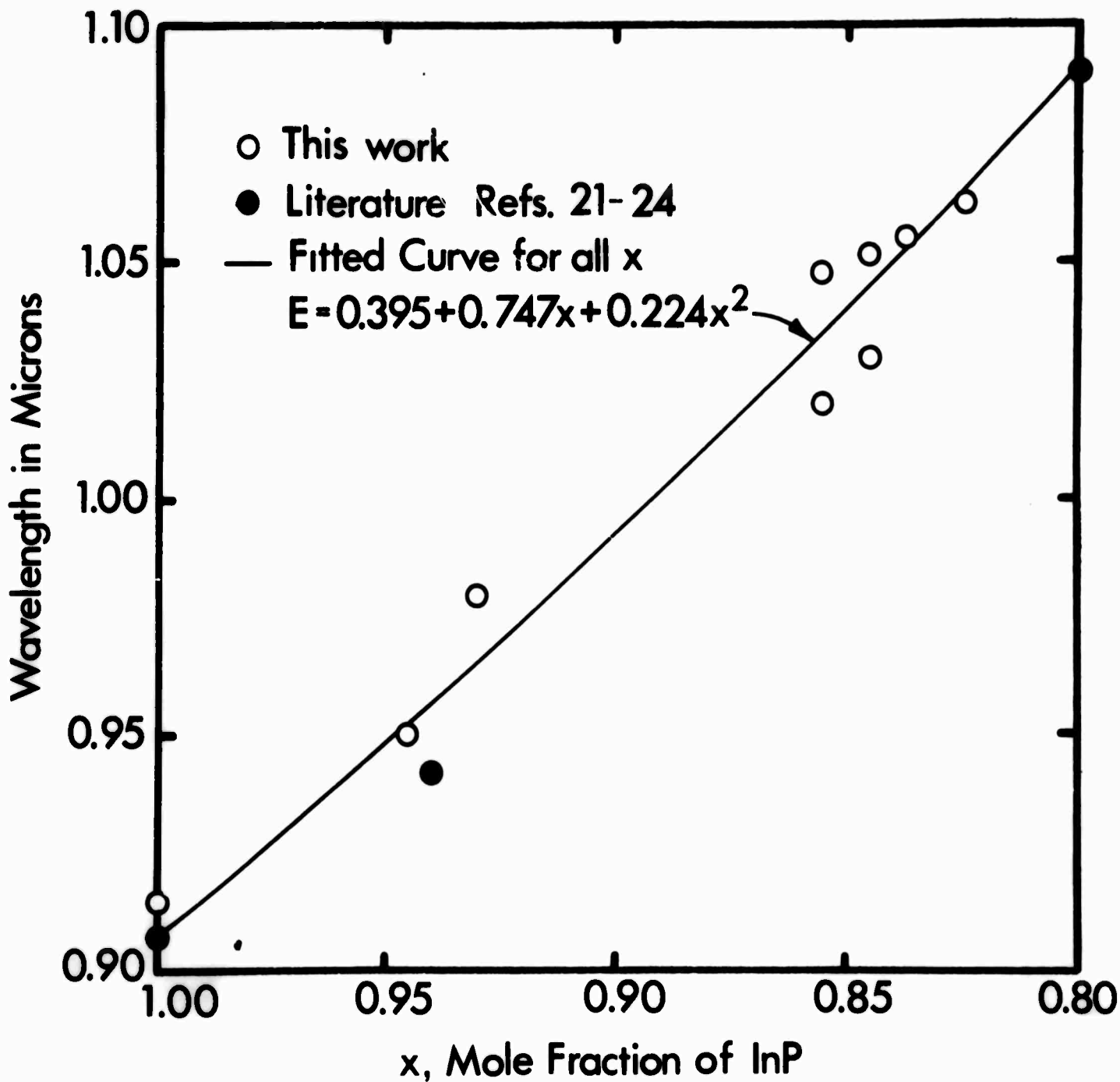


Figure 16. Variation of Wavelength of Light Emitted from  $\text{InAs}_{1-x}\text{P}_x$  Laser Diodes at  $77^\circ\text{K}$

The "C" value of 0.224 compares very favorably with recent theoretical work by Van Vechten and Bergstresser,<sup>26</sup> who obtained 0.23 for the same coefficient.

## 6. OPTICAL AMPLIFICATION EXPERIMENT

### (a) Diode Selection

An experiment was performed to determine whether optical gains could be achieved by coupling an InAsP injection laser to a neodymium-glass amplifier. Diodes were selected to fall close to the desired  $1.06\mu$  wavelength and to have reasonable outputs (typically 25 - 100 milliwatts). The experiment was done at the Central Research Laboratory of American Optical Company in Southbridge, Massachusetts.

### (b) Glass-Fiber Amplifier Design

The optically pumped amplifier was a glass fiber consisting of an alkaline earth, silicate-glass host containing approximately 5 weight percent neodymium oxide. The amplifier was designed as a dielectric waveguide such that only the lowest order  $HE_{11}$  mode is propagated along the fiber.<sup>27,28</sup> The equivalent spontaneous input power to the amplifier is given by

$$P = 2\Delta v N \epsilon_{ph} \text{ watts}$$

where  $\Delta v$  is the linewidth of the amplified spontaneous emission in hertz,  $N$  is the number of propagating modes, and  $\epsilon_{ph}$  is the energy per photon.<sup>29</sup> The factor of 2 arises from the assumption that two polarization states exist per mode. Since the input noise is proportional to the square root of the mode number  $N$ ,<sup>30</sup> the lowest input noise will be realized when the

mode number is held down to one propagating mode. For radiation with a wavelength of  $1\mu$  and a  $100\text{\AA}$  bandwidth, this results in a spontaneous input power of  $1.2\mu\text{W}$  per mode. For single mode ( $\text{HE}_{1,1}$ ) propagation, the condition

$$2.405 > \frac{\pi d}{\lambda} \sqrt{n_1^2 - n_2^2}$$

must be satisfied. This relation specifies diameter ( $d$ ) and index of refraction of the fiber-amplifier core ( $n_1$ ) and cladding ( $n_2$ ). The second fused cladding on the glass-fiber amplifier consisted of samarium glass. This glass is transparent to the pump radiation while serving as an absorber for  $1.06\mu$  radiation. The diameter of the fiber core was  $15\mu$  ( $n_1 = 1.5638$ ); the first cladding diameter,  $45\mu$  ( $n_2 = 1.5630$ ) and the overall diameter approximately  $3\text{mm}$ . The length of the fiber was  $45\text{cm}$  with the ends beveled at  $20$  degrees in order to suppress feedback and self-oscillation. The peak wavelength of the amplifier used was  $1.0610\mu$ . Substituting these values into the condition for lowest mode propagation gives a value less than  $2.405$  (2.28).

The specific-gain coefficient for  $\text{Nd}^{3+}$  in the glass has the same wavelength dependence as the spontaneous emission. The peak of the spontaneous emission and its linewidth are functions of the host-glass compositions. Figure 17 shows typical fluorescent curves for  $\text{Nd}^{3+}$  in various readily made glasses. The peak position of the fluorescence can be varied over a

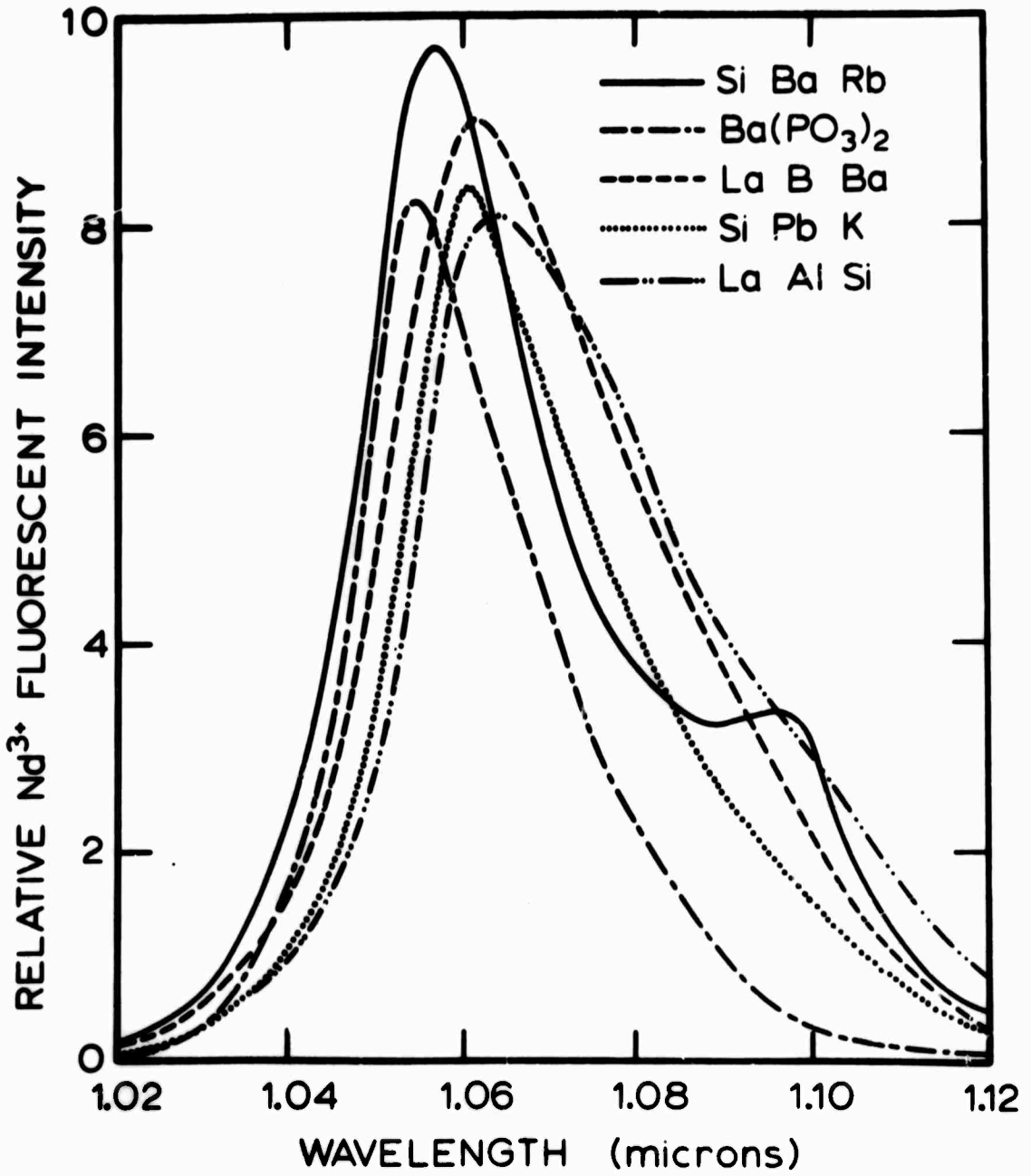


Figure 17. Spontaneous Emission Spectral Envelopes for Nd<sup>3+</sup> in Various Host Glasses

wavelength interval of  $100\text{\AA}$  and the linewidth (one-half-intensity points) at room temperature varies from  $245$  to  $380\text{\AA}$ . A particularly simple and well-behaved family of laser glasses is the barium potassium silicates; in Table 4 the position of the peak wavelength, the linewidth, and the lifetime of fluorescence for changes in the barium and potassium content are given.

(c) Experimental Arrangement

The experimental arrangement for the detection of amplification of the injection-laser emission is shown in Figure 18. The InAsP injection laser is mounted on a copper heat sink extending into a liquid nitrogen Dewar flask. The emitted radiation exits through an unsilvered stripe on the Dewar glass walls and enters the microscope objective, having  $5\times$  magnification and a numerical aperture (NA) of  $0.20$ . A beam splitter and eyepiece allow observation of the injection-laser die. The injection-laser emission is then focused upon a gimbal-mounted mirror optimized for  $1.06\mu$  reflection. The diverging beam is refocused on the fiber-amplifier entry face by another  $5\times$  NA  $0.20$  microscope objective. A final  $5\times$  NA  $0.20$  objective is located at the exit face of the fiber laser providing a near-parallel beam of the amplified light, which passes through a  $1.06\mu$  spike filter and is incident on the photocathode of the photomultiplier detector.

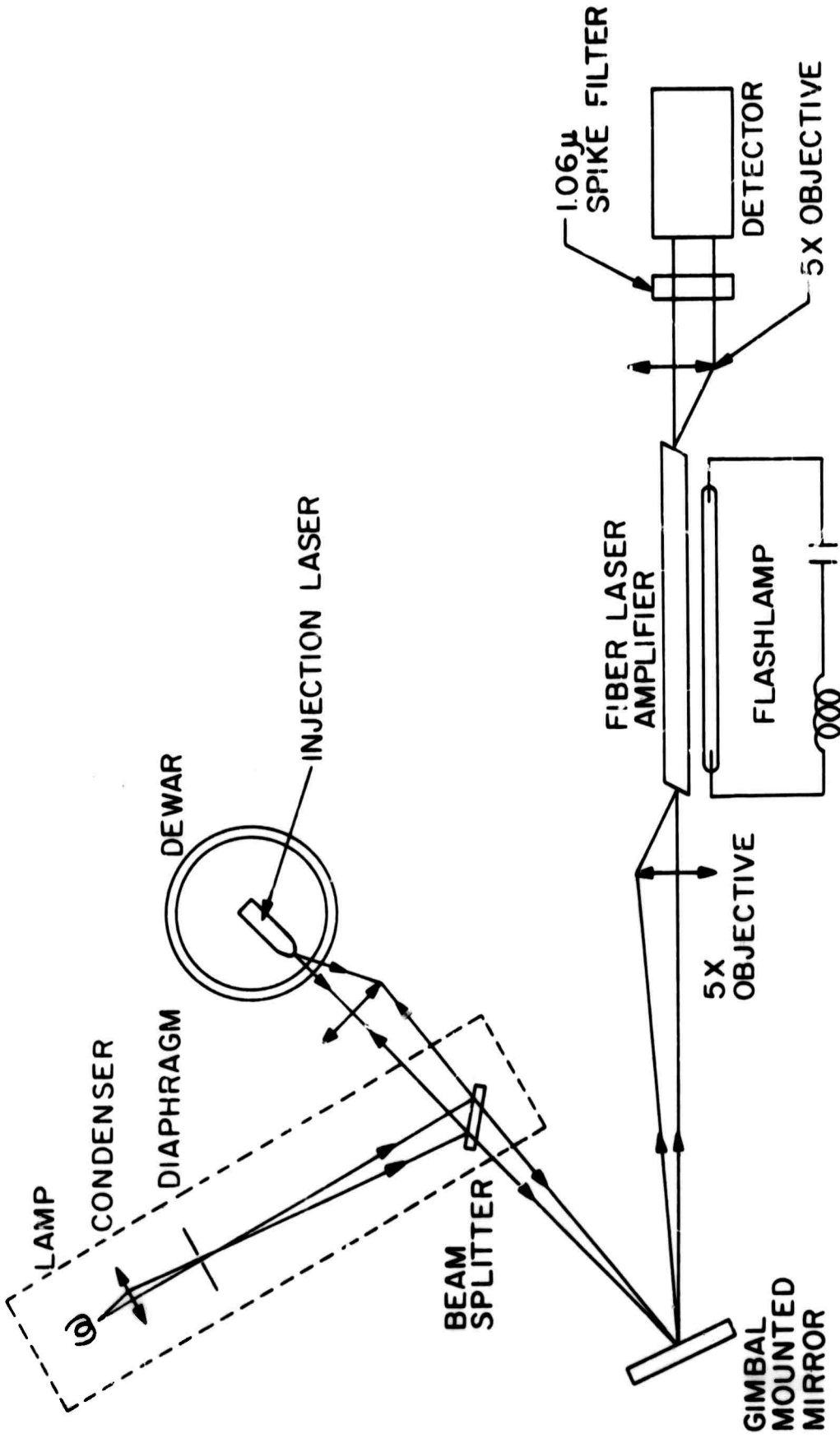
The fiber laser is pumped with a xenon-arc flash lamp. The whole

TABLE 4\*

<u>X</u>	<u>Y</u>	<u><math>\tau</math> Measurement (ms)</u>	<u>Peak Wavelength <math>\lambda(\mu)</math></u>	<u>Linewidth <math>\Delta\lambda</math> (nm)</u>
25	5	0.64	1.0605	29.0
20	10	0.72	1.059	28.5
15	15	0.74	1.058	27.5
10	20	0.78	1.057	25.5
5	25	0.77	1.056	26.5

\* Composition 69.5 weight percent  $\text{SiO}_2$ , 0.5  $\text{Nd}_2\text{O}_3$ ,

X BaO and Y  $\text{K}_2\text{O}$ .



**Figure 18. Experimental Arrangement for Optical Amplification of Injection Laser Emission**

arrangement is placed on a granite slab for stability. The major difficulty in the experiment was to provide the alignment necessary to allow a significant portion of the  $1.06\mu$  injection laser emission to impinge upon the glass-fiber core. The alignment procedure was as follows. All optical elements were first visually aligned, and adjusted so that their center lines lay in a plane parallel to the surface of the granite table. The injection laser was positioned so that the cone of the emitted radiation was incident upon the first microscope objective. By use of a vertical illuminator attachment, which is shown enclosed by dashed lines in Figure 18, the front surface of the laser crystal could be sufficiently illuminated to provide an easily recognized image on a diffuse screen placed over the center of the gimbal-mounted mirror. The glass-fiber amplifier was similarly imaged upon the mirror by replacing the detector with a light source. The image of the glass-fiber core was then superimposed upon the image of the injection-laser crystal in the approximate position of the lasing junction. Final adjustments were made by using the InAsP laser as the active element, all components being placed in accordance with Figure 18, and looking for output from the photomultiplier while making tiny angular adjustments on the mirror. When the signal was acquired, fine translational, angular, and focusing adjustments provided order-of-magnitude improvements in signal output. Care had to be taken to prevent the saturation of the photomultiplier by scattered light from the flash lamp pump.

Attempts to utilize the glass-fiber amplifier as the active element and to use the injection laser as a photovoltaic detector with a thin lamina of active volume were unsuccessful. This was probably due to the relatively low impedance of the injection laser devices.

(d) Results

The injection laser pulse, as it is received in the photomultiplier after transmission through the unpumped glass fiber, is shown in Figure 19(a). For this exposure, as well as during the rest of the experiment, the injection current peak was 15 amperes ( $1.4 \times 10^4$  A/cm<sup>2</sup>), resulting in a total laser output of approximately 80 mW. The photomultiplier, operated at 1.5 kV, gave a peak output of approximately 1.5 volt pulse height across a 1 k $\Omega$  load resistance. The RC time constant of the photomultiplier circuit can be seen in the decay time of the pulse. Figure 19(b) shows the fluorescence emission from the fiber under pumped conditions. The flash lamp energy was 226 joules at 1.8 kV. The photomultiplier gain was decreased by reducing the total dynode voltages to 700 volts.

Since the stimulated gain is a maximum at the peak of spontaneous emission, the injection laser pulse was delayed until the time of peak fluorescence emission. Figure 20(a) shows the oscilloscope synchronized to the injection laser pulse that occurs 700  $\mu$ s after the initiation of the flash lamp pump. Since the horizontal scale in this photograph is

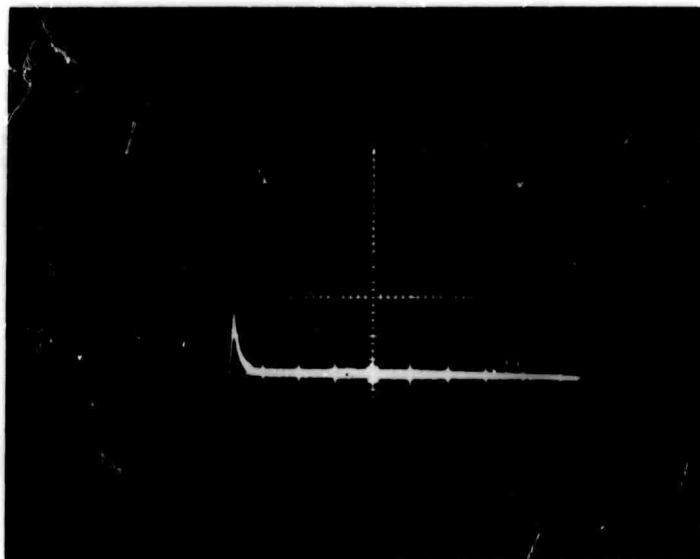


Figure 19a. Light Pulse from Injection Laser.

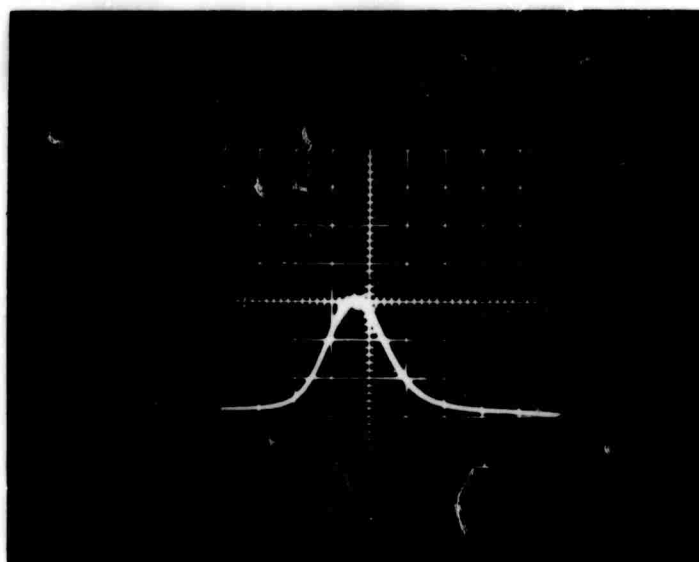
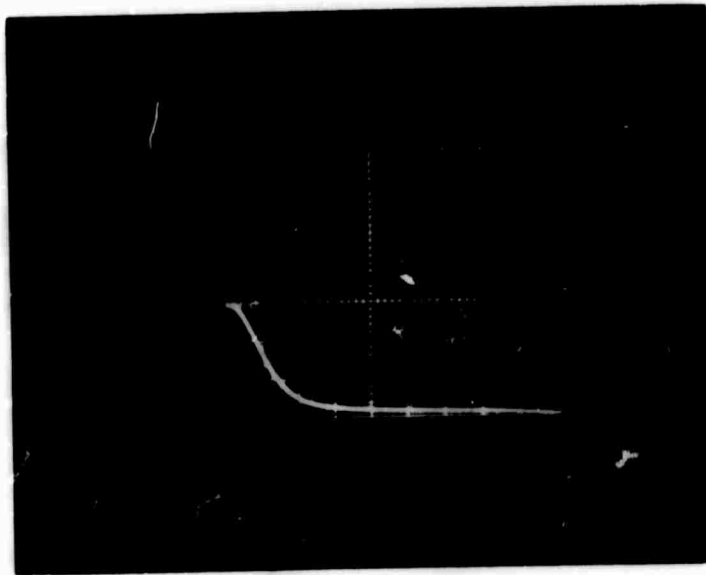
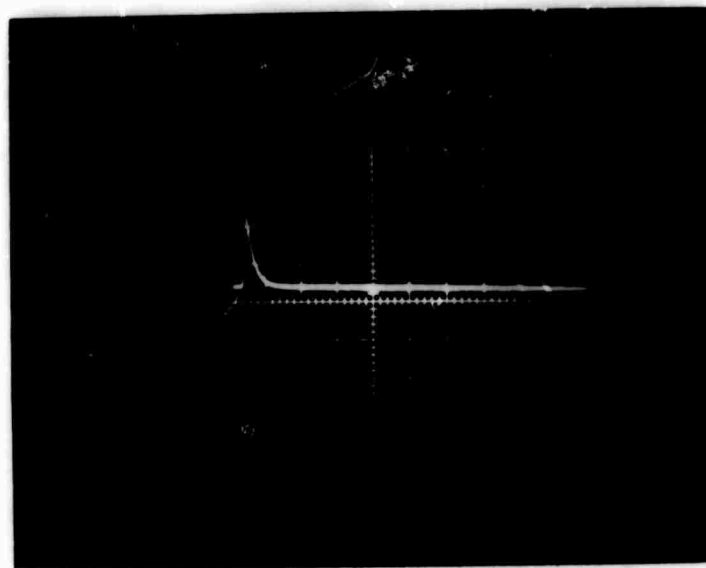


Figure 19b. Fluorescence from Optical Amplifier



**Figure 20a. Optical Amplifier Output 700  $\mu$ sec  
After Pump Initiation**



**Figure 20b. Optically Amplified Injection Laser  
Pulse on Crest of Fluorescence  
Emission**

200  $\mu\text{s}/\text{div.}$ , the injection laser pulse is compressed sufficiently so that it can not be seen. Figure 20(b) shows the amplified injection laser pulse riding on the maximum of the spontaneous emission peak with a time scale equivalent to that used in the initial photograph (1  $\mu\text{s}/\text{div.}$ ). In the entire series of experiments, the flash lamp driven amplifier was operated on a single pulse basis.

Experiments were run to observe gain as a function of injection pulse delay time, and as a function of pump energy. Photomultiplier current saturation was prevented by the use of stacked neutral density glass plate filters that attenuated the optical signal. The gain was defined as the signal amplitude from the output end of the glass fiber in the pumped versus the unpumped condition. The maximum gain was measured as  $5.7 \times 10^4$  or 47 dB. The amplified signal was three times larger than the amplified spontaneous emission and could be easily separated from the latter. The emitted noise is due to the fluctuations in spontaneous emission and its magnitude depends upon the bandwidth.<sup>28</sup> For a pulse duration of 100 nanoseconds, the input noise amplitude is  $10^{-8}$  watt or less.

An injection laser emission of 4  $\mu\text{W}$  was coupled into the propagating  $\text{HE}_{11}$  mode of the fiber core. The attenuation of the injection laser emission by approximately  $10^3$  is mainly attributed to geometrical factors, such as scattering of the light by condensation on the Dewar glass walls, and

poor imaging of the light emitting surface of the injection laser within the diameter of the glass fiber amplifier core.

Heating effects in the glass fiber amplifier caused some variation in gain. This was attributed to spontaneous line broadening as a function of temperature, which could have a beneficial effect if the injection laser wavelength was slightly off the spontaneous wavelength peak.

(e) Conclusions

A peak gain of 47 dB was realized when an InAsP injection laser was optically mated to a glass fiber amplifier. Further optimization of these injection laser structures at higher carrier concentration leads to the expectation of greater power outputs and higher temperature operation. Further optimization of the optical coupling into larger cross section and longer fibers promises multiwatt outputs from similar systems and kilowatt outputs are feasible with the addition of rod amplifiers. The above work was recently published.<sup>31</sup>

## 7. CONCLUSIONS

$\text{InAs}_{1-x}\text{P}_x$  ingots have been grown by the Czochralski technique having a tailored composition. Materials studies on boat-grown InP yielded much useful information on electrical properties, distribution coefficients, etc. on this little-studied compound. A pseudobinary phase diagram quite different from that given by previous workers was established for the InAs-InP system. The distribution coefficients of major impurities in and electrical properties of the alloys were measured.

Diffusion experiments were carried out particularly establishing parameters at one alloy composition and temperature. The diodes were prepared by a specially developed polishing procedure applied to a matrix of arbitrarily oriented grains rather than the usual cleaving of oriented slices.

Laser diodes fabricated from the  $\text{InAs}_{1-x}\text{P}_x$  ingots gave up to 0.5W output at better than 1% overall efficiency under pulsed conditions at temperatures of approximately 100°K. The spectral output of these lasers occurred close to 1.060 microns, and could be fine-tuned by changing the operating temperature slightly.

A wide variation in properties between individual diodes and from ingot to ingot was to be expected under the circumstances. However, several

of the ingots used gave diodes that had over 100 mW output. Attempts to correlate this output, the efficiency or threshold with factors such as dopant type or concentration were inconclusive.

An experiment carried out to demonstrate coupling of a  $1.06\mu$  laser diode with a Nd-doped glass fiber was highly successful. The diode emission was coupled into the fiber through microscope optics. The fiber was optically pumped and a maximum gain of approximately 50,000 observed. The way is therefore open for the investigation of practical modulated high-power systems using  $\text{InAs}_{1-x}\text{P}_x$  diode lasers efficiently coupled into Nd-doped glass or YAG amplifier rods.

The main aspects of the program have been realized. Further real improvement in the development of the devices awaits the preparation of single crystal material. Then the diffusion phenomena, contacts and laser variations can be studied in the most optimum manner. At the present time variations in grain size, orientation and perhaps other properties overshadow the expected effects. It is felt that the InAs-InP system has real promise for a number of reasons. The ability to dope with n-type impurities to well over  $10^{19} \text{ cm}^{-3}$  gives much lower resistivities than are attainable in GaAs without formation of precipitates.

Single crystal material of  $\text{InAs}_{1-x}\text{P}_x$  is a very definite requirement,

and will probably be attained by pulling from stoichiometric melts under high pressure, using the liquid encapsulant method. Further development along the lines used in GaAs should give less Joule heating in the contacts and improved devices. Thus CW operation at 77°K and pulsed operation at room temperature have to be regarded as very real and immediate possibilities for  $\text{InAs}_{1-x}\text{P}_x$  1.06 $\mu$  laser diodes.

8. REFERENCES

1. R. K. Willardson, A. G. Thompson and B. Ross, ONR Technical Report, Contract N00014-68-C-0219, (Nov. 1968), AD 679 908.
2. R. Gremmelmaier, Z. Natur. 11A, 511 (1956).
3. E. P. A. Metz, R. C. Miller and R. Mazelsky, J. Appl. Phys. 33, 2106 (1962).
4. J. B. Mullin, B. W. Straugham and W. S. Brickell, J. Phys. Chem. Solids 26, 782 (1965).
5. J. W. Wagner and R. K. Willardson, Trans. Met. Soc. AIME 242, 366 (1968).
6. R. K. Willardson and W. P. Allred, p. 35, Proc. Conf. on GaAs, Reading, 1966 (Inst. Phys. and Phys. Soc., London, 1967).
7. M. Glicksman and K. Weiser, J. Electrochem. Soc. 105, 728 (1958).
8. R. C. Clarke, B. D. Joyce and W. H. E. Wilgoss, Solid State Comm. 8, 1125 (1970).
9. R. K. Willardson, "Lattice Defects in Semiconductors," R. R. Hasiguti, Ed., p. 221 (Univ. of Tokyo Press and Penn. State Univ. Press, 1968).
10. "Compound Semiconductors," Vol. 1, R. K. Willardson and H. L. Goering, Eds., pp 158 and 390 (Reinhold, New York, 1962).
11. M. R. Lorenz and S. E. Blum, J. Electrochem. Soc. 113, 559 (1966).
12. "Semiconductors and Semimetals," Vol. 2, R. K. Willardson and A. C. Beer, Eds., p. 73 (Academic Press, New York, 1966).
13. M. E. Straumanis, J. P. Kramme and M. Rubenstein, J. Electrochem. Soc. 114, 640 (1967).
14. A. G. Thompson, J. E. Rowe and M. Rubenstein, J. Appl. Phys. 40, 3280 (1969).
15. W. Köster and W. Ulrich, Z. Metallkunde 49, 365 (1958).
16. J. Steininger, J. Appl. Phys. 41, 2713 (1970).

17. H. Robbins and B. Ross, J. Electrochem. Soc. 117, 97C (1970).
18. K. A. Arseni, B. I. Boltaks and T. D. Dzhaforov, Phys. Stat. Solid. 35, 1053 (1969).
19. L. L. Chang and H. C. Casey, Solid State Elec. 7, 481 (1964).
20. C. D. Dobson, Brit. J. Appl. Phys. 17, 187 (1966).
21. I. Melngailis, Appl. Phys. Letts. 2, 176 (1963).
22. K. Weiser and R. S. Levitt, Appl. Phys. Letts. 2, 178 (1963).
23. F. B. Alexander et al, Appl. Phys. Letts. 4, 13 (1964).
24. N. G. Basov et al, Sov. Phys. Tech. Phys. 12, 250 (1968).
25. A. G. Thompson and J. C. Woolley, Can. J. Phys. 45, 255 (1967).
26. J. A. VanVechten and T. K. Bergstresser, Phys. Rev. B1, 3351 (1970).
27. E. Snitzer, J. Opt. Soc. Am. 51, 491 (1961).
28. E. Snitzer and H. Osterberg, J. Opt. Soc. Am. 51, 499 (1961).
29. R. J. Glauber in "Physics of Quantum Electronics," P. L. Kelley, B. Lax and P. E. Tannewald, Eds., p. 788, McGraw-Hill, New York (1966).
30. G. C. Holst and E. Snitzer, IEEE J. Quant. Elec. QE-5, 319 (1969).
31. B. Ross and E. Snitzer, IEEE J. Quant. Elec. QE-6, 366 (1970).

UNCLASSIFIED

Security Classification

DOCUMENT CONTROL DATA - R & D		
<i>(Security classification of title, body of abstract and indexing annotation must be entered when the overall report is classified)</i>		
1. ORIGINATING ACTIVITY (Corporate author) BELL & HOWELL ELECTRONIC MATERIALS DIVISION 360 Sierra Madre Villa Pasadena, California 91109		2a. REPORT SECURITY CLASSIFICATION <b>UNCLASSIFIED</b>
3. REPORT TITLE  INDIUM ARSENIDE-PHOSPHIDE INJECTION LASERS		2b. GROUP
4. DESCRIPTIVE NOTES (Type of report and inclusive dates) Final Technical Report, June 1969 - August 1970		
5. AUTHOR(S) (First name, middle initial, last name)  Alan G. Thompson, Bernd Ross		
6. REPORT DATE October, 1970	7a. TOTAL NO. OF PAGES 72	7b. NO. OF REFS 31
8a. CONTRACT OR GRANT NO. N00014-69-C-0415	8b. ORIGINATOR'S REPORT NUMBER(S)  6	
8c. PROJECT NO. DEFENDER	8d. OTHER REPORT NO(S) (Any other numbers that may be assigned this report)  ---	
10. DISTRIBUTION STATEMENT This document has been approved for public release and sale; its distribution is unlimited.		
11. SUPPLEMENTARY NOTES  ---	12. SPONSORING MILITARY ACTIVITY OFFICE OF NAVAL RESEARCH Physics Branch Arlington, Virginia 22217	
13. ABSTRACT  The indium arsenide-phosphide alloy system has been studied. Indium arsenide and indium phosphide compounds were prepared by pulling and directional freezing respectively. The InP ingots were characterized for distribution coefficients and electrical properties. Ingots of $\text{InAs}_{1-x}\text{P}_x$ were pulled by two modifications of the Czochralski technique--an all-quartz sealed system and pulling through a liquid encapsulant. The two methods are compared and the latter found to be superior for these alloys. Electrical, X-ray and mass spectrometric measurements were made on the alloy ingots. Laser diodes were fabricated in a similar manner to those reported on previously, with power outputs up to 0.5W at $1.06\mu$ with better than 1% efficiency being obtained under pulsed conditions close to $100^\circ\text{K}$ . Amplification of the $1.06\mu$ emission from an $\text{InAs}_{1-x}\text{P}_x$ laser diode was demonstrated in a Nd-doped glass fiber, showing a system gain of 50,000.		

DD FORM 1473  
1 NOV 65REPLACES DD FORM 1473, 1 JAN 64, WHICH IS  
OBSOLETE FOR ARMY USE.

UNCLASSIFIED

Security Classification

10. KEY WORDS	LINK A		LINK B		LINK C	
	ROLE	WT	ROLE	WT	ROLE	WT
Crystal Growth						
Liquid Encapsulation						
Indium Arsenide						
Indium Phosphide						
Indium Arsenide-Phosphide						
Pseudobinary Phase Diagram						
Alloys						
Distribution Coefficients						
Transport Properties						
Semiconductors						
Lasers						
Injection Lasers						
Light Amplification						